1965

A measurement of dead space and its effect on the homogeneous nucleation rate of water vapor in helium

Michael A. Grayson

A MEASUREMENT OF DEAD SPACE AND ITS EFFECT ON THE HOMOGENEOUS NUCLEATION RATE OF WATER VAPOR IN HELIUM

BY

MICHAEL A. GRAYSON, 1941

AN

ABSTRACT

submitted to the faculty of the

UNIVERSITY OF MISSOURI AT ROLLA

in partial fulfillment of the requirements for the

Degree of

MASTER OF SCIENCE IN PHYSICS

Rolla, Missouri

1965

A MEASUREMENT OF DEAD SPACE AND ITS EFFECT ON THE HOMOGENEOUS NUCLEATION RATE OF WATER VAPOR IN HELIUM

The existence of a "dead space" surrounding each nucleated water droplet is demonstrated and measurements of its rate of development are made. The effects of this "dead space" are considered to be due to both the removal of vapor from the helium-water vapor mixture and the evolution of heat about the drop due to its growth. The results confirm the usefulness of the concept of a "dead space" and provide a means for its measurement with respect to time. Recommendations for further study and a method of correcting for dead space effects is given.

A MEASUREMENT OF DEAD SPACE AND ITS EFFECT ON THE HOMOGENEOUS NUCLEATION RATE OF WATER VAPOR IN HELIUM

BY

MICHAEL A. GRAYSON

A

THESIS

submitted to the faculty of the

UNIVERSITY OF MISSOURI AT ROLLA

in partial fulfillment of the requirements for the

Degree of

MASTER OF SCIENCE IN PHYSICS

Rolla, Missouri

1965

Approved by

James L. Kassner, Jr. (advisor) Otto H. Hill

Charles E. Antle

J. Rhoads

ACKNOWLEDGEMENTS

The author wishes to thank his advisor, Dr. James L. Kassner, Jr., for the encouragement, advice, and assistance extended by him during the course of this research.

Thanks are due to the author's co-researchers, Mssrs. Louis B. Allen, Ronald Dawbarn, Donald S. Packwood, Raymond J. Schmitt, and John C. Carstens for their suggestions and help in setting up the cloud chamber and reducing the data. Gratitude is also expressed to Miss Cheryl Mueller and Mssrs. Robert Madding, Frank Ollinger, and Brunn Roysden for their contributions to this work. Thanks are due to Mr. Lee N. Anderson of the Mechanical Engineering Department for his fine machine work, Mr. Carl Lund for his work on computer programming, and Mssrs. Herbert Alcorn and Donald Byrd of the Computer Science Center for their help in seeing the computer program to success.

Thanks are due also to my wife, Margaret, for her patience in translating my drafts into English.

This research was supported by the Atmospheric Sciences Section of the National Science Foundation, NSF Grant GP-2893.

TABLE OF CONTENTS

		Page
ACKNOWLEDGEMENTS		ii
LIST OF FIGURES		iv
LIST OF TABLES		v
LIST OF PLATES		vi
I.	INTRODUCTION	1
	1. Homogeneous Nucleation	1
	2. Statement of the Problem	2
II.	THE THEORY	5
	1. Liquid Drop Theory of Homogeneous Nucleation	5
	2. The Exponential Factor	6
	3. Evaluation of the Kinetic Coefficient	9
	4. Droplet Growth Theory	17
III.	THE CLOUD CHAMBER	23
	1. Supersaturation	23
	2. Homogeneous Nucleation	25
	3. Sensitive Time	25
	4. The Basic Cloud Chamber Experiment	27
	5. Analyzing Photographic Data	30
IV.	THE EXPERIMENT	32
	1. An Illustration of Dead Space	32
	2. A Theoretical Analysis of the Wire Experiment	33
	3. Double Pulse Expansions	39
	4. Mathematical Analysis	43
	5. Other Details of the Experiment	45
V.	CONCLUSIONS	51
	1. Dead Space per Unit Volume	51
	2. Vapor Depletion	51
	3. Further Work	53
	BIBLIOGRAPHY	55
	APPENDIX A	57
	APPENDIX B	66
	VITA	68

LIST OF FIGURES

Figure		Page
1.	Nucleation rate laws	16
2.	Geometry of diffusion problem	17
3.	Growth of drop radius in a supersaturated system	19
4.	Measure of sensitive time for spiked pulse expansion	26
5.	Example of the ideal pressure trace and examples of operational pressure traces for cloud chamber expansions	29
6.	Supersaturation profile for the wire in helium.	37
7.	Supersaturation profile for the wire in argon .	38
8.	Drop density profile for the wire in helium . .	40
9.	Drop density versus the peak supersaturation for single pulse expansions	41
10.	Example of double pulse expansion	42
11.	Comparison of D(t) and diffusion models of dead space about a drop	46
12.	Dead space per drop versus time	48
13.	Supposed dead space curve compared to measured dead space curve	49
14.	Percent dead space versus time	52

LIST OF TABLES

Table Page

I. List of homogeneous nucleation rate laws. . . . 14

LIST OF PLATES

Plate — Page

1. Dead space of wire in helium. 34
2. Dead space of wire in argon. 35

CHAPTER I

INTRODUCTION

The formation of clouds in the earth's atmosphere is governed by the large number of foreign particles present in suspension in the air. These particles afford convenient centers for natural condensation. Such condensation is the subject of Fletcher's[1] heterogeneous nucleation theory. This theory is based on the theory of homogeneous nucleation, thus a comprehensive understanding of the processes of homogeneous nucleation should serve well in promoting an understanding of all forms of nucleation.

1. Homogeneous Nucleation. Wilson[2] was among the first to observe homogeneous nucleation in cloud chambers. Volmer[3] conceived a physical mechanism which allowed him to calculate a theoretical homogeneous nucleation rate. Extensions of Volmer's approach have appeared over the last three decades. Many of these theoretical attacks are based on the liquid drop model in which very small droplets, representing the initial fragments of the new phase, are assumed to have the well-defined thermodynamic properties of the bulk liquid phase. Starting from this point, the theories give a homogeneous nucleation rate law which possesses the following general form:

$$J = A \exp \left[\frac{-B}{(\ln S)^2}\right], \qquad (1\text{-}1)$$

where J is the number of drops formed/cm^3-sec and S is the supersaturation. The quantities A and B may be functions of temperature, pressure, and supersaturation. For the range of supersaturations studied experimentally, about 4.3 to 5.8, the quantities A and B may be considered as constant. The $1/(\ln S)^2$ term dominates the changes in B and the exponential dominates the changes in A. In the work below, A and B will then be considered as constant factors.

The theory predicts an increase by a factor of 10^2 in the nucleation rate with an increase of 5% in supersaturation. As a result, experimenters have made determinations of the "critical supersaturation," i.e. the minimum supersaturation required to produce a barely observable quantity of droplets during a cloud chamber expansion. Such measurements can only provide an approximate determination of the temperature dependence on the critical supersaturation. Frey attempted to measure the increase in the nucleation rate as a function of supersaturation. It was apparent that droplet growth effects dominated his experiment.[4]

2. Statement of the Problem. To advance our understanding of the nucleation process, experimental techniques must be employed which are capable of discerning the firm details of the theories. Experimental techniques in current usage measure the combined effects of nucleation and droplet growth.

A means of discerning the way in which the growth of a droplet perturbs the region immediately adjacent to it is needed. Such information would offer a means of correcting experimental measurements of the nucleation rate for the effects of droplet growth. Courtney[5] calculates the rate of droplet growth. However, he assumes a uniform vapor distribution throughout the volume and neglects the evolution of heat from the droplets. Such procedures are only justified for the crudest sort of analysis.

Allard and Kassner[6] developed a technique for making precise measurements of the combined effects of nucleation and droplet growth. They described a technique for correcting the measurements for the effects of droplet growth which turned out to be somewhat impractical due to the limitations of the apparatus.

The concept of "dead space" surrounding a growing droplet appears to be the most realistic and practical means of taking droplet growth effects into account. This "dead space" is defined as the volume surrounding a drop in which no further nucleation occurs as a result of: 1) removal of water molecules from the vapor by the growing drop, 2) evolution of the latent heat of condensation from the droplet.

This work describes a technique which allows the approximate measurement of the dead space around a growing droplet as a function of its age. This data will provide

a means of correcting measured nucleation rates so that these can be properly compared with nucleation theory.

CHAPTER II

THE THEORY

Theoretical approaches to the physics of nucleation vary in both model and result. A brief review of the theoretical treatments of homogeneous nucleation will be given along with some theoretical treatments of droplet growth. Much is to be gained by such a review as it shows how widely diversified the theories are and it provides a meaningful basis for a detailed discussion of some aspects of the physics of nucleation. A convenient terminus for all theoretical nucleation treatments is the nucleation rate. This relates the number of drops formed/cm^3-sec as a function of the supersaturation.

1. Liquid Drop Theory of Homogeneous Nucleation. A basic starting point for many of these theories is the liquid drop model. The assumptions made are: 1) the first fragments of the condensed phase are well-defined liquid droplets which have the bulk properties of the liquid, 2) once nuclei are formed and become free growing, they are imagined to be removed from the system and re-inserted as monomers.

All of the liquid drop theories agree to the general form of the rate law:

$$J = A \exp\left[\frac{-B}{(\ln S)^2}\right] , \qquad (2\text{-}1)$$

where A and B are quantities to be considered as constant, and S is the supersaturation. The kinetic coefficient, A, is on the order of 10^{23} sec^{-1}-cm^{-3} depending upon the means by which it is derived. The exponential factor, B, is generally on the order of 10^{2} and may be a function of temperature. In this work the temperature is taken at a constant value.

The nucleation rate is very sensitively dependent upon the supersaturation through the exponential term so that a small change in S, say from 4.7 to 5.0, results in a large change in J, say from 50 drops/cm^3-sec to several thousand drops/cm^3-sec.

2. The Exponential Factor. An analysis of the results of various theoretical treatments shows that the constant, B, in Eq. (2-1) is the same. Farley's[7] development of the quantity B will be given here.

A system is initially at a temperature T and pressure P. The system contains one liquid drop with g molecules and radius r. If m is the mass of one molecule and ρ is the density of the bulk liquid, then the relation,

$$mg = 4/3\pi r^3\rho \ , \qquad (2\text{-}2)$$

follows directly. If ϕ_a is the Gibbs free energy per molecule of the vapor phase and ϕ_b is the Gibbs free energy per molecule of the liquid phase, then the free energy ϕ_g of the liquid drop of g molecules may be written as:

$$\phi_g = (\phi_b - \phi_a)g + 4\pi r^2\sigma \ , \qquad (2\text{-}3)$$

where σ is the surface tension. The last term arises because the molecules in the surface do not have a full complement of interacting molecules on all sides. Eq. (2-2) may be expressed as follows,

$$4\pi r^2\sigma = \left[\frac{3\sigma(4/3)^{1/3}\pi^{1/3}m^{2/3}}{\rho^{2/3}}\right] g^{2/3} . \quad (2-4)$$

Considering the quantity in brackets as a constant, C, Eq. (2-4) becomes,

$$4\pi r^2\sigma = Cg^{2/3} . \quad (2-5)$$

Making this substitution in Eq. (2-3), one obtains,

$$\phi_g = (\phi_b-\phi_a)g + Cg^{2/3} . \quad (2-6)$$

When the vapor is undersaturated, ϕ_a is less than ϕ_b, consequently the free energy is monotonic increasing with g. However, when the vapor is supersaturated, ϕ_a is greater than ϕ_b and the free energy passes through a maximum at $g = g^*$. In a supersaturated vapor, clusters of size g^* will become free growing (nucleate) with the addition of a single molecule, or evaporate with the removal of a single molecule. At $d\phi/dg = 0$, $g = g^*$ and clusters of size g^* are in equilibrium with the vapor. Thus

$$\phi_b - \phi_a = -2/3\ Cg^{*-1/3} = \frac{-8\pi\sigma r^{*2}}{3g^*} , \quad (2-7)$$

where r^* is the radius of a cluster of size g^*. Substituting Eq. (2-7) into Eq. (2-3) gives the free energy at equilibrium:

$$\phi_{g^*} = 4/3\ \pi\ r^{*2}\sigma . \quad (2-8)$$

It is helpful to consider clusters of size less than g^* to be embryos, clusters of size g^* to be nuclei, and clusters of size greater than g^* to be free-growing droplets.[8] In essence, the nucleation rate concerns itself with the rate at which nuclei are formed. Thus, knowledge of the distribution of cluster sizes from $g = 1$ to $g = g^*$, or greater, is necessary. In order to maintain a tractable rate theory, the equilibrium distribution of cluster size, N_g, is assumed adequate. If N_0 is the number of monomers per unit volume, then kinetic theory gives N_g as:

$$N_g = cN_0 \exp(-\phi_{g*}/kT) = cN_0 \exp\left[\frac{-4\pi r^{*2}\sigma}{3kT}\right], \qquad (2\text{-}9)$$

where c is a constant.

The Kelvin equation[9] gives the equilibrium condition between the cluster and the vapor:

$$RT\ln S = 2M\sigma/\rho r, \qquad (2\text{-}10)$$

where T is absolute temperature,

R is the gas constant,

M is the molecular weight of the liquid,

ρ is the density of the bulk liquid,

S is the supersaturation,

r is the cluster radius.

An expression for r is obtained from this equation

$$r = \frac{2M\sigma}{\rho RT\ln S} \quad . \qquad (2\text{-}11)$$

If Eq. (2-11) is substituted into Eq. (2-9), the result is

$$N_g = cN_0 \exp\left[\frac{-16\pi\sigma^3 M^2}{3kR^2T^3\rho^2} \quad \frac{1}{(\ln S)^2}\right],$$

where the B factor of Eq. (2-1) is recognized to be

$$B = -\frac{16\pi\sigma^3 M^2}{3kR^2T^3\rho^2} . \qquad (2\text{-}12)$$

Although this is the generally accepted theoretical expression for the B factor, both theoreticians and experimenters realize that this result has some obvious short-comings due to the fact that σ and ρ are normally taken as bulk values. The justification for the use of bulk values in describing nuclei of such small size is dubious.

Work has been done both in theory and experiment to determine corrected values of σ for droplets of 200 Å diameter or less in both saturated and supersaturated atmospheres.[10,11,12]

3. Evaluation of the Kinetic Coefficient. The following discussion outlines some of the techniques employed by various theoretical investigators for evaluating the kinetic coefficient, A.

Becker and Döring[13] use the same approach outlined in the preceding section for determining the exponential factor. The kinetic coefficient is evaluated by considering the condensation process to involve a series of quasi-chemical reactions which take a cluster from the g-mer to

(g+1)-mer. Assuming a stationary distribution of cluster sizes in the vapor, the nucleation process may be considered as a series of slow reactions through the distribution of cluster sizes. Assigning a probability for the evaporation of a molecule from a cm^2 of surface in time dt, and a similar probability for the condensation of a molecule, Becker and Döring postulate a current flowing through the distribution of cluster sizes. A system of equations are set up which are analogous to Ohm's law. The nucleation process is considered to be a series of resistances through which the nucleation rate J flows as a current between the potential difference represented by the droplet surface. This mathematical artifice allows the kinetic coefficient to be evaluated; the result is shown in Table I.

The Becker-Döring treatment is set forth clearly by Schmitt.[14] Becker and Döring maintain that their method gives some insight into the significance of the kinetic coefficient which other workers, namely Farkas,[15] overlook.

Zeldovich[16] derives a rate law which is equivalent to that of Becker and Döring except for the factor, γ, the so-called Zeldovich factor, which accounts for the fact that the system may depart from the equilibrium distribution of cluster sizes due to the steady state current. Table I shows the result of his calculation.

Farkas[15] evaluates the kinetic coefficient by assuming the classical liquid drop hypothesis and considering the effect of collisions of vapor molecules with the clusters. The number of molecules in a given cluster is assumed to fluctuate in a fashion similar to the movement of Brownian particles in a force field. The ratio of the number of clusters of size g+1 to the number of size g is obtained and is identified as a differential form of the nucleation rate. The nucleation rate J is thereby a function of clusters of g and g+1 molecules and the corresponding probabilities for condensing or evaporating a single molecule from these clusters. This system of differential equations is then approximated by a single differential equation which is solved with appropriate boundary conditions. Becker and Döring[13] maintain that the undetermined constant, c (shown in Table I), in the Farkas theory should have been identified as the total surface area of all the monomer molecules.

Sander and Damköhler[17] perform a series of experiments to test the temperature dependence of the Becker and Döring theory. They measure the critical supersaturation for homogeneous nucleation over the greatest possible temperature range, from +35° C to -75° C. Although offering a nucleation rate law, they do not show explicitly the steps taken to evaluate the kinetic coefficient. They indicate the use of the same starting point as Becker and Döring[13]

and Volmer[3] but perform a somewhat more exact calculation. As can be seen in Table I, this results in a correction of the B factor as well as the A factor of the general rate law. Using their own rate law, Sander and Damköhler are able to plot a nucleation rate curve that falls between that given by Becker and Döring and Volmer.

Volmer[3] first establishes the B factor, in the same fashion as given in paragraph 2 above. By considering that all drops, which exist in the vapor, pass through a critical size in the process of their growth, the critical size is pictured as a narrow gate to the process of nucleation. Obviously, the nucleation rate must be proportional to the number of drops of critical size existing in the vapor at any instant in a state of unstable equilibrium; i.e. proportional to exp $\left[-B/(\ln S)^2\right]$.

Assuming, as do others, that once a drop becomes free growing it is removed from the system and replaced by single water vapor molecules, equal in number to those contained in the free growing drop, he maintains that the nucleation rate is the product of the number of such drops and the number of single molecules of the vapor striking the surface of such a critical size drop per unit time. Taking an expression for the number of vapor molecules striking a unit area per unit time from kinetic theory, he obtains the result given in Table I. This method of attack is one of the earliest and many authors have modified this

basic approach.

Frenkel[18] discusses the theoretical works of Volmer[3] and Becker and Döring[13] in some detail. He proceeds to derive an expression for the velocity of condensation (nucleation rate) from a purely kinetic argument, rejecting the thermodynamic concepts which lead to the theories of Volmer and Farkas.[15] His argument closely parallels that of Becker and Döring in that he starts with a detailed microscopic balancing of clusters of molecules going from size n to clusters of n+1 and n-1 molecules. Becker and Döring consider this balancing condition to lead to an equilibrium distribution of clusters. Frenkel follows Zeldovich[16] and assumes the balancing condition results in a simple non-equilibrium distribution of clusters. By continuing his analysis in the same vein as Becker and Döring and Zeldovich, he arrives at the rate law presented in Table I. Farley[7] goes through similar arguments to obtain the result for the A factor listed below.

The works in Table I are listed by author. The last column shows the number of drops nucleated cm^{-3}-sec^{-1} at a supersaturation of 5.0, and a final temperature of -5.0° C. The meaning of the various quantities in the A and B factors is given on the page following Table I.

AUTHOR	"A" FACTOR	"B" FACTOR	J in drops/cm^3-sec at S = 5.0
BECKER and DÖRING[13]	$\frac{2 Z_1 P_1 \sigma M N_o O_1}{3 R^2 T^2 g \rho \ln S} \sqrt{\frac{2\sigma N_o}{\pi M}}$	$\left(\frac{\sigma}{T}\right)^3 \left(\frac{M}{\rho}\right)^2 \frac{16\pi N_o}{3R^3}$	7.42×10^3
ZELDOVICH[16]	$\gamma \frac{2 Z_1 P_1 \sigma M N_o O_1}{3 R^2 T^2 g \rho \ln S} \sqrt{\frac{2\sigma N_o}{\pi M}}$	$\left(\frac{\sigma}{T}\right)^3 \left(\frac{M}{\rho}\right)^2 \frac{16\pi N_o}{3R^3}$	$\gamma 7.42 \times 10^3$
FARKAS[15]	$C \frac{P_1 \rho R T (\ln S)^2}{16 \pi \sigma^2 M} \sqrt{\frac{2\sigma N_o}{\pi M}}$	$\left(\frac{\sigma}{T}\right)^3 \left(\frac{M}{\rho}\right)^2 \frac{16\pi N_o}{3R^3}$	$C\, 1.58 \times 10^1$
VOLMER[3]	$\frac{16 Z_1 P_1 \sigma^2 M^2 N_o \pi g}{(\rho R T \ln S)^2 \sqrt{2\pi M R T}}$	$\left(\frac{\sigma}{T}\right)^3 \left(\frac{M}{\rho}\right)^2 \frac{16\pi N_o}{3R^3}$	2.97×10^3
FRENKEL[18]	$\frac{8 Z_1 P_1 \sigma^2 M^2 N_o \pi}{(\rho R T \ln S)^2} \sqrt{\frac{g \ln S}{3 M R T}}$	$\left(\frac{\sigma}{T}\right)^3 \left(\frac{M}{\rho}\right)^2 \frac{16\pi N_o}{3R^3}$	4.28×10^5
FARLEY[7]	$\frac{Z_1 P_1 M}{R T \rho} \sqrt{\frac{2\sigma N_o}{\pi M}}$	$\left(\frac{\sigma}{T}\right)^3 \left(\frac{M}{\rho}\right)^2 \frac{16\pi N_o}{3R^3}$	1.13×10^3
SANDER and DAMKÖHLER[17]	$\frac{Z_1 P_1 \sigma M N_o O_K}{3 R^2 T^2 g \rho \ln S} \sqrt{\frac{2\sigma N_o}{\pi M}}$	$\left[\left(\frac{\sigma}{T}\right)^3 \left(\frac{M}{\rho}\right)^2 \frac{16\pi N_o}{3R^3}\right]\left[1 - \frac{4}{g^{2/3}} + \frac{2}{g}\right]$	1.10×10^5

TABLE I

where Z_1 is the number of water molecules/unit volume,

P_1 is the vapor pressure of the liquid immediately after the expansion but before condensation,

M is the molecular weight,

σ is the surface tension,

N_0 is Avogadro's number,

S is supersaturation,

R is the gas constant,

T is absolute temperature,

g is the number of molecules in drops of critical size,

ρ is density,

O_K is the surface area of spherical water molecule in droplet embryos,

O_1 is the surface area of spherical water molecule in vapor phase,

γ is the Zeldovich factor,

c is the proportionality constant.

The results tabulated in Table I have been reduced to the desired form by the author for comparison purposes. In some cases the way they appeared in the literature obscured the heavy dependence upon S. The form presented here is convenient for numerical calculations. Fig. 1 shows some of these theoretical rate laws along with Schmitt's empirical rate law. Appendix B shows the values used for calculating the constants A and B along with the values found for A and B.

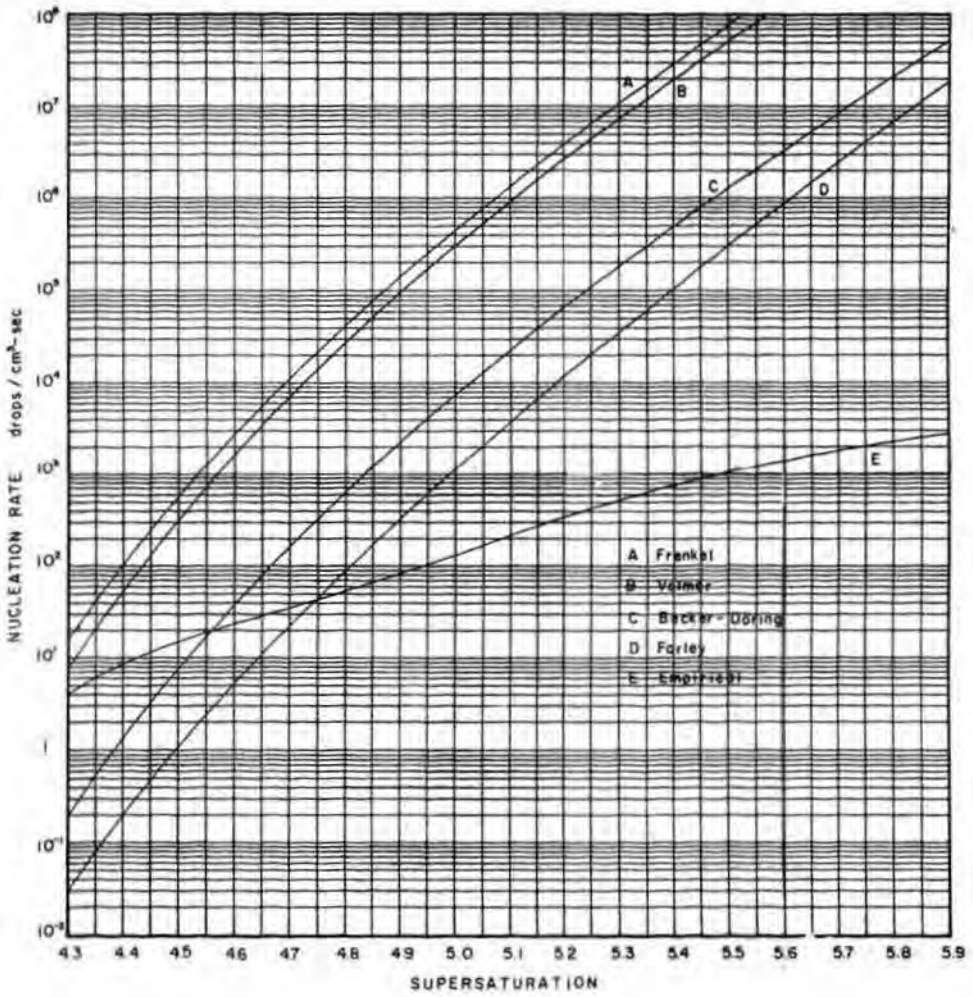
NUCLEATION RATE drops / cm³-sec
SUPERSATURATION
4.3 4.4 4.5 4.6 4.7 4.8 4.9 5.0 5.1 5.2 5.3 5.4 5.5 5.6 5.7 5.8 5.9
A
B
C
D
E
A Frenkel
B Volmer
C Becker - Döring
D Farley
E Empirical

FIGURE I

4. Droplet Growth Theory. A brief review of work on droplet growth is in order to provide sufficient background for the work to follow.

Bagge, Becker, and Bekow[19] start by considering condensation as a quasi-stationary diffusion problem. Obviously, for the drop radius R to increase, vapor must diffuse to the drop surface and condense. The equation for the increase of drop mass per unit time yields:

$$dm/dt = \rho\, 4\pi r^2\, dr/dt = 4\pi r^2 D \left[\partial \rho(r)/\partial r\right]_{r=R} , \quad (2\text{-}13)$$

where ρ is the density of the bulk liquid, the variable $\rho(r)$ is the existing vapor density in the vicinity of the drop, and D is the diffusion coefficient of the vapor molecule in the supporting gas. Assuming the diffusion equation to be an accurate description of the case, the density distribution about the drop is regulated so that $\rho(r)$ obeys

$$\nabla \rho(r) = 0 . \quad (2\text{-}14)$$

Fig. 2 shows the geometry of the problem and the pertinent variables.

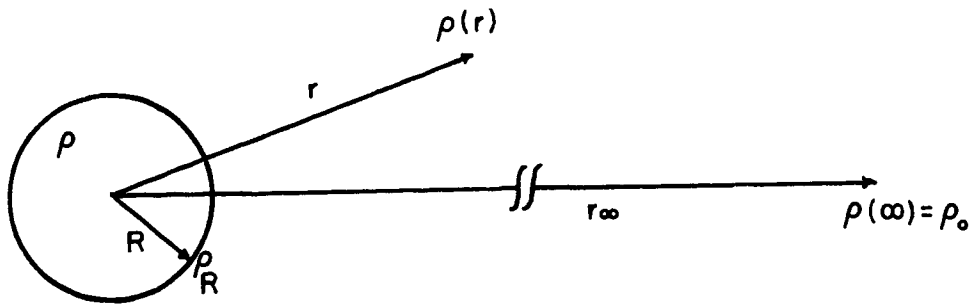

FIGURE 2

Boundary conditions for the system are:

$$\rho(r) = \rho_R \quad \text{at } r = R$$

$$\rho(r) = \rho_0 \quad \text{at } r = \infty \ .$$

Applying these boundary conditions to the general solution of Eq. (2-14), one has:

$$\rho(r) = \rho_0 - \frac{R}{r}\left[\rho_0 - \rho_R\right] \quad . \tag{2-15}$$

From Eqns. (2-13) and (2-15) the increase in drop radius per unit time follows:

$$dR/dt = \frac{D\rho_0}{\rho}\,\frac{1}{R}\left[1 - \frac{\rho_R}{\rho_0}\right] \quad . \tag{2-16}$$

Taking $\rho(R) \cong \rho_\infty$ where ρ_∞ is the equilibrium saturation vapor pressure and directly integrating Eq. (2-16), gives

$$R^2 = \frac{2D\rho_0}{\rho}\left[1 - \frac{\rho_\infty}{\rho_0}\right] t \quad , \tag{2-17}$$

where $\rho_0 / \rho_\infty = S$. Fig. 3 shows the drop radius as a function of time for various supersaturations.

The authors consider the possibility that warming of the drop due to condensation may cause a decrease in its growth rate. They arrive at an equation for the temperature difference between the drop and its environment. This modification supports the very slow droplet growth rate observed experimentally by these authors.

The author uses Eq. (2-13) in a computer program designed to keep up with the droplet growth during a cloud

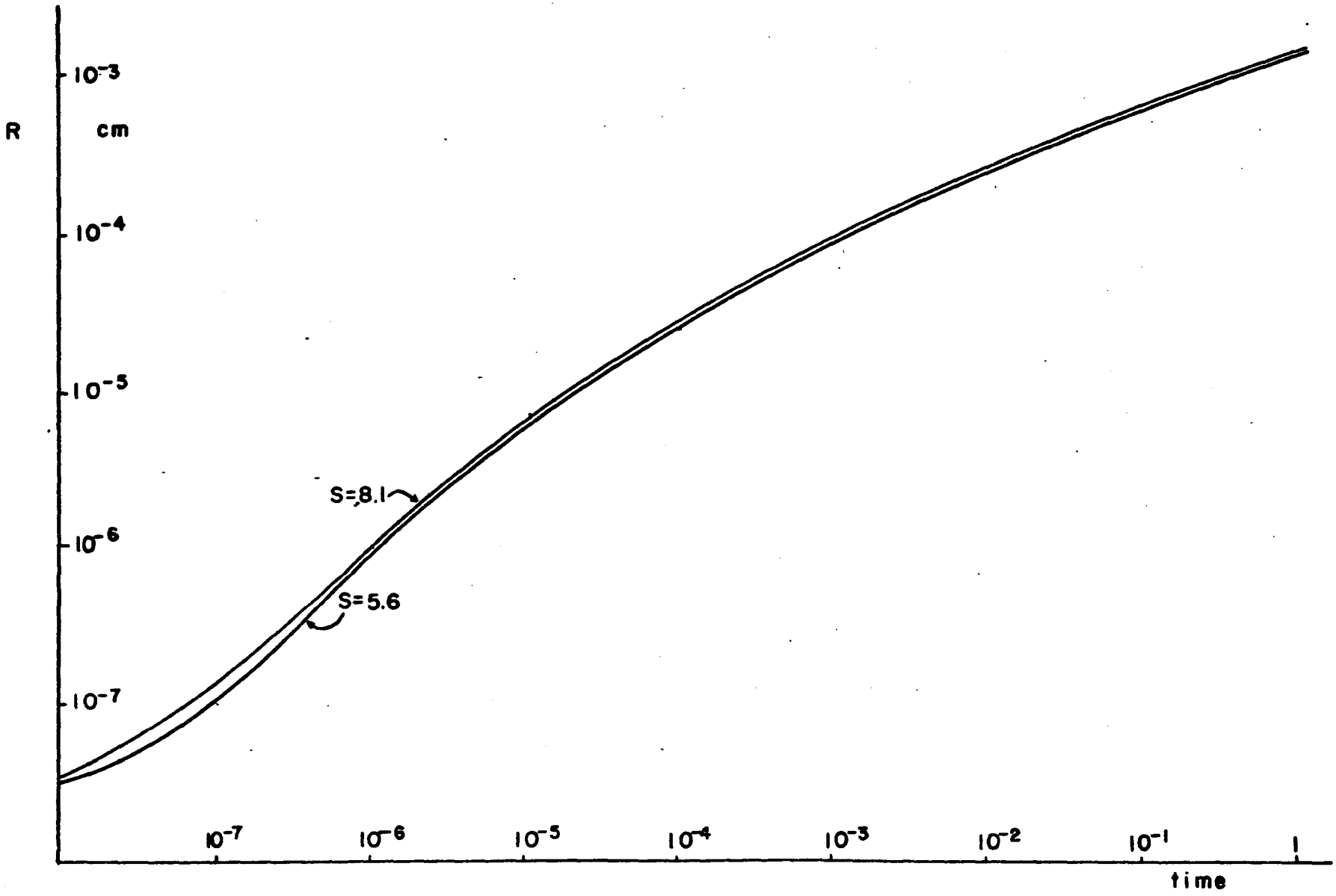
R
cm
10^{-3}
10^{-4}
10^{-5}
10^{-6}
10^{-7}
S=8.1
S=5.6
10^{-7}
10^{-6}
10^{-5}
10^{-4}
10^{-3}
10^{-2}
10^{-1}
1
time

FIGURE 3

chamber expansion where nucleation is taking place. By using Eq. (2-13) the maximum possible rate of droplet growth is represented. This gives the rate of removal of vapor molecules from the system. If one now smears out the effects of vapor depletion by assuming a uniform vapor distribution, the uniform vapor density may be adjusted for the depletion of vapor and a new homogeneous nucleation rate calculated. Thus, this somewhat unrealistic model may be utilized as a simple means of keeping track of the nucleation rate as a function of the time during a nucleation experiment. Further detail is given in Appendix A.

Courtney[5] presents a somewhat different attack on the problem. Assuming a collision-frequency growth law, the net mass M depositing per second onto a cluster of g molecules with surface area S_g may be written as:

$$(dM/dt)_{cluster} = mS_g \left[\alpha_g uc - \alpha_g{}^r u^r\right], \qquad (2\text{-}18)$$

where m is the mass of a depositing molecule,

α_g is the accomodation coefficient for condensation,

$\alpha_g{}^r$ is the accomodation coefficient for evaporation,

u is the collision frequency per unit area for deposition from the vapor actually present per unit concentration of vapor,

u^r is the collision frequency per unit area for deposition from the vapor at equilibrium,

c is the actual concentration of vapor present,

S_g is the surface area of a cluster.

The concentration of water vapor in equilibrium with a plane surface, assuming α_g and $\alpha_g{}^r$ do not change with concentration, is then given by,

$$C_E = (\alpha_g{}^r u^r)/(\alpha_g u) . \qquad (2\text{-}19)$$

Substituting this result in Eq. (2-18) gives,

$$(dM/dt)_{cluster} = \alpha_g um(c - C_E)S_g . \qquad (2\text{-}20)$$

The author goes on to show that,

$$(dM/dt)_{cluster} = d(\rho 4\pi r^3/3)/dt = S_g \rho\, dr/dt . \qquad (2\text{-}21)$$

The combination of Eqns. (2-20) and (2-21) yields,

$$dr/dt = (\alpha_g um/\rho)(c - C_E) . \qquad (2\text{-}22)$$

Integrating the last equation from t' to t gives the radius r(t) of a drop. Assuming that the radius of the cluster is negligible compared to its radii at later times when the cluster becomes the size of a drop, one has:

$$r_t = (\alpha_g um/\rho)\int_{t'}^{t}(c - C_E)dt , \qquad (2\text{-}23)$$

where t' evidently is employed to avoid ambiguities occurring at the initial stages of growth.

Courtney then continues in an effort to incorporate this result into Frenkel's rate law. This work is tedious and not of general use here.

Compared to the work of Bagge, Becker, and Bekow[19] the results are similar but not identical. Courtney's treatment is presented in the language of chemical kinetics whereas Bagge, Becker, and Bekow set the problem up as a macroscopic diffusion problem.

Any effort to make precise measurements of homogeneous nucleation rates is hampered by the fact that droplet growth commences as soon as a droplet is nucleated. And for measurements of nucleation that are made over a finite length of time, as are all experimental observations, droplet growth and the thermodynamic and hydrodynamic perturbations incurred have an effect that has hitherto not been examined in detail. Schmitt[14] minimized the effects of droplet growth in his measurements by performing experiments in which droplets were nucleated for very short lengths of time, on the order of 0.015 seconds for 90% nucleations. This author intends to concentrate on that effect which Schmitt minimized in hopes that this information will prove useful in correcting experimental measurements of homogeneous nucleation rates.

CHAPTER III

THE CLOUD CHAMBER

The Cloud Chamber is a valuable tool in nucleation studies since cloud chamber data may be used to easily calculate supersaturations and nucleation rates.

1. Supersaturation. Supersaturation is the ratio of the vapor density immediately after the expansion but before condensation to the equilibrium vapor density at the final temperature of the expansion.[20] Schmitt[14] shows that the supersaturation may be calculated from the expression,

$$S = \frac{p_I}{p_F} \frac{P_F}{P_I} , \qquad (3\text{-}1)$$

where p_I is the equilibrium vapor pressure at the initial temperature previous to expansion,

p_F is the equilibrium vapor pressure at the final temperature after the expansion,

P_I is the initial absolute pressure,

P_F is the final absolute pressure.

Both P_F and P_I are directly measurable quantities with the instrumentation available on the U. M. R. Cloud Chamber. The vapor pressures p_I and p_F are direct functions of the temperature and values of p_I and p_F are given in the International Critical Tables[21] for the temperature range encompassed in an expansion. The initial temperature,

which is known, enables determination of p_I. The final temperature, which may be calculated by means of the adiabatic law,

$$T_I P_I^{\frac{1-\gamma}{\gamma}} = T_F P_F^{\frac{1-\gamma}{\gamma}} \quad , \qquad (3\text{-}2)$$

enables determination of p_F.

It has been shown by Allard[22] that the expansion chamber can be programmed to a constant supersaturation for about 0.5 seconds after the expansion in the center of the chamber. Studies in this work require that the chamber maintain S constant for less than 0.5 sec. Possible error in the calculation of S may arise from three sources: 1) the initial temperature, 2) the initial and final pressures, and 3) the adiabatic index used in Eq. (3-2). The error in final temperature is implicit in the last two considerations above. If the pressures are measured to 0.5 mm of Hg, the initial temperature is known to 0.05° K and the adiabatic index for the helium-water vapor mixture taken to be accurate in the third decimal place, then the supersaturation may be in error by $\pm$ 1/10. An analysis of the operating characteristics of the cloud chamber has been carried out by Packwood.[23] It can be concluded from the work of Allard,[22] Schmitt,[14] and Packwood[23] that sufficient precision and accuracy are possible to allow nucleation rates to be measured to

within ± 10%. Definitions of several other terms used commonly in cloud chamber research should be made here.

2. Homogeneous Nucleation. Homogeneous nucleation may be defined as spontaneous formation of droplets of the mother phase independently of foreign centers of nucleation, such as dust particles. Homogeneous nucleation is dependent mainly upon the degree of supersaturation attained by the system.

3. Sensitive Time. The definition of sensitive time, T_0, as used here is very specialized. As shown by Schmitt,[14] the data which is obtained from the U. M. R. Cloud Chamber may be best interpreted by computing the supersaturation at a series of points on the pressure spike. Then by integrating in a discrete fashion an empirical nucleation rate curve over the time varying curve, the total number of droplets nucleated can be determined and compared with that which is observed. Due to the nature of the general form of the rate law, more nucleation occurs at the peak of the pressure spike than along the sides. The sensitive time, which is a measure of the time that the cloud chamber is at a supersaturation high enough to cause homogeneous nucleation, shall be defined as that width of the spike which includes 90% of the drops formed using the method of numerical integration given by Schmitt. Fig. 4 illustrates this concept a little more meaningfully.

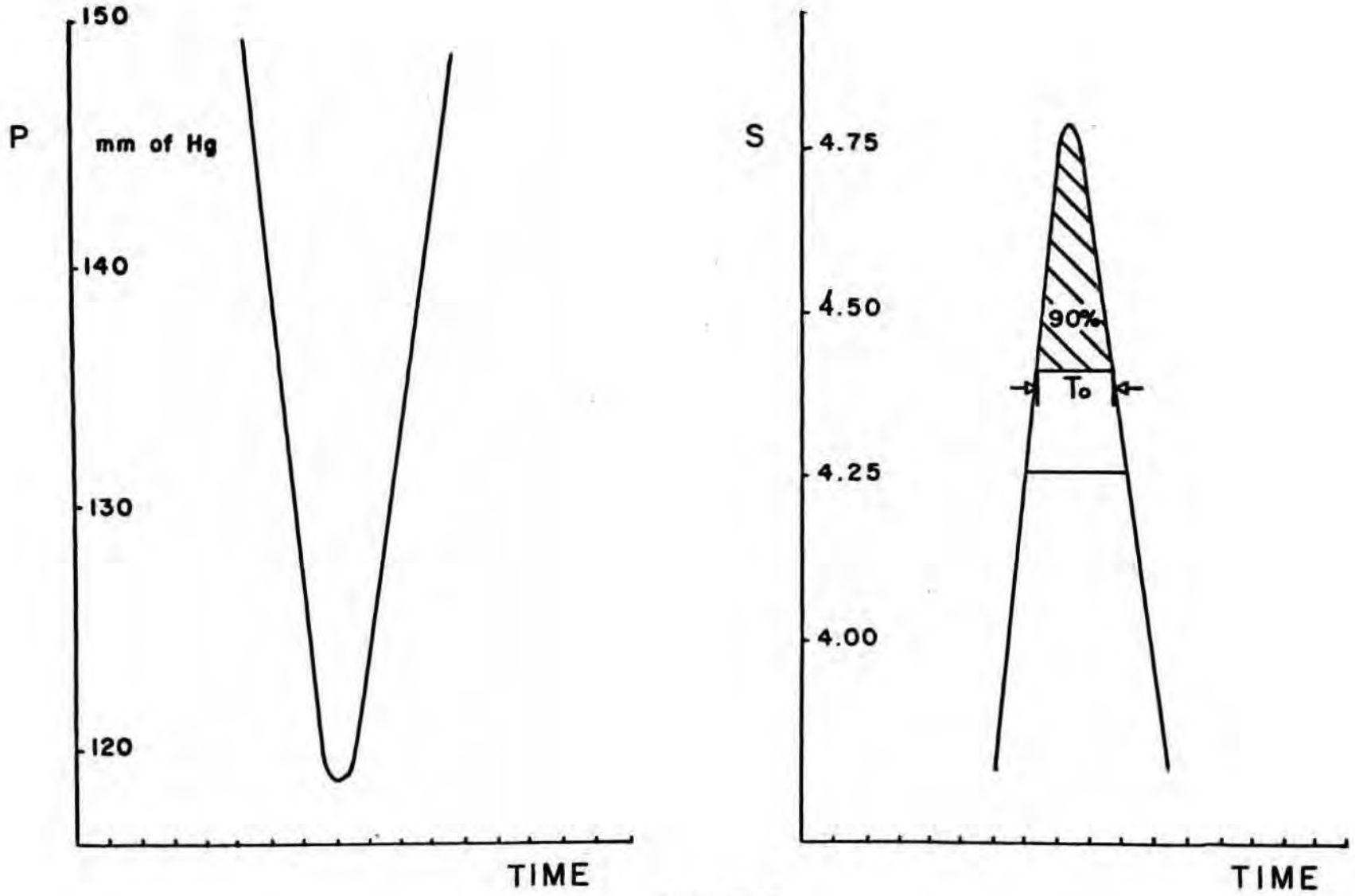

FIGURE 4

4. The Basic Cloud Chamber Experiment. The Cloud Chamber used at the University of Missouri at Rolla is a necessarily complex instrument but basically it performs a very simple function. Allard[22] gives a detailed explanation of its operation.

A cloud chamber experiment consists of an expansion of the interior volume of the chamber, known as the sensitive volume. The pressure of the sensitive volume is monitored by a solid state pressure transducer thus allowing a very sensitive measure of the pressure at any time during the expansion. The piston is maintained at some arbitrary ready position where the initial temperature and pressure readings are taken. The piston is then allowed to drop a set amount which may be controlled by the timing circuits. This results in an expansion of the sensitive volume which occurs in about 0.05 seconds. The pressure circuit measures the initial pressure, turns "off" during the bulk of the expansion itself, and then turns "on" again to measure the pressure for a time near the end of the expansion. Several expanded scales are employed.

Since compressive heating effects tend to compress the sensitive volume shortly after the expansion, a series of slow expansion valves are normally used at this point. These may be set to compensate exactly for the compressive heating effect, thus resulting in a steady final pressure trace from the transducer. It has been found that the

piston and the mass of water above it tend to oscillate, since they are trapped between two gases. These oscillations are of such a magnitude as to make the final pressure oscillate with an amplitude of several inches of water. This destroys the possibility of defining a final constant supersaturation, thereby making it impossible to perform the square pulse expansion envisioned by Allard and Kassner.[6] Fig. 5-A shows the ideal square pulse and Fig. 5-B the type of square pulse obtained due to oscillations.

Schmitt[14] avoided this difficulty by making use of the first spike resulting from the oscillations. Instead of staying at the pressure of the system at the end of the expansion, a compression valve was turned on for a very short time. This resulted in a final pressure trace which very nearly approximated a parabola. The sensitive volume was recompressed just enough to take it below the critical supersaturation so that the oscillations did not affect the cloud chamber during the time allowed for droplets growing to photographable size. Fig. 5-C shows the type of pressure trace resulting from this type of expansion. The author makes use of this same technique since it provides data which may be interpreted with ease in comparison to that shown in Fig. 5-B.

The basic cloud chamber experiment then yields the initial pressure, the initial temperature, the final

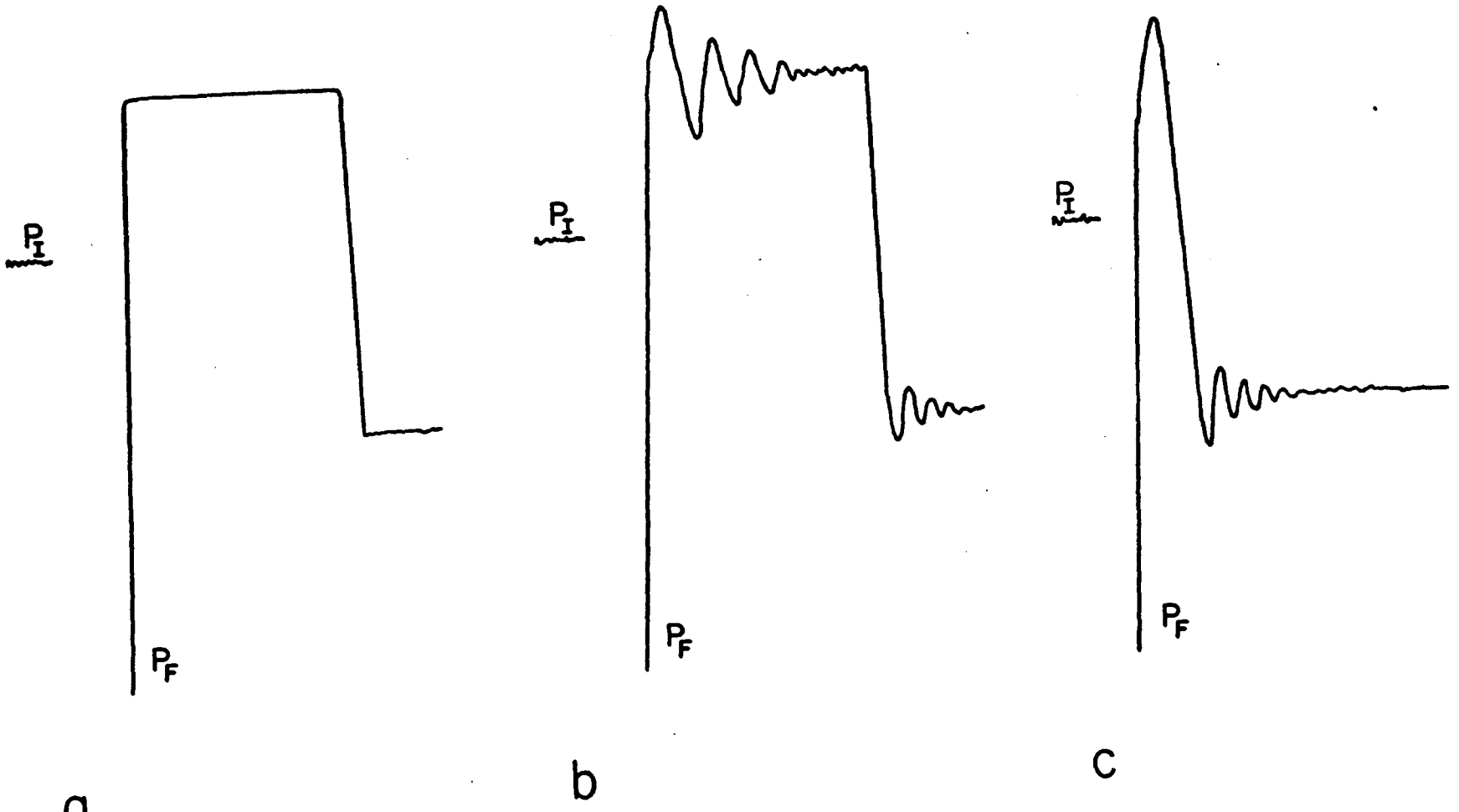

FIGURE 5

pressure, and a photograph of the resulting droplet population as data. As shown above, with the help of the International Critical Tables and the adiabatic law, the supersaturation may be calculated from this information. Since the parabolic pulse expansion does not have a constant final pressure, as does a square pulse expansion, the supersaturation may be calculated for a number of points along the parabolic pulse providing a time varying curve of supersaturation. This is the P_0/P_∞ employed in the work of Bagge, Becker, and Bekow,[19] Eq. (2-17) of this work.

5. Analyzing Photographic Data. In order to gather useful information from an expansion it is necessary to know how many drops formed in the sensitive volume. About two hundredths of a second after the parabolic pulse expansion, the nuclei formed in that pulse have grown to a size large enough that they may be seen. At this time a sequence of three stereoscopic photographs are begun. The technique of photography is explained in detail by Allard[22] and Schmitt.[14] From the pictures taken during the expansion, the number of drops formed per cm^3 may be obtained by projecting the negative on a screen which is divided into squares of such a size that they represent a cubic centimeter of the sensitive volume when the width of the illuminating beam is taken into consideration. From these drop counts one may determine the nucleation rate by

multiplying the drop count by $1/T_0$ for that expansion.

Thus, the cloud chamber is a tool capable of giving the information necessary to study nucleation rate laws, namely the supersaturation and the nucleation rate.

CHAPTER IV

THE EXPERIMENT

There are many ways in which the dead space may be investigated experimentally. After considerable discussion amongst the cloud-chamber group, two promising experiments were attempted. The first experiment gives a physical picture of the dead space, the second provides a means of measuring its growth.

1. An Illustration of Dead Space. The concept of a dead space surrounding free growing drops may at first seem rather nebulous. A simple experiment may be performed to show that such a dead space indeed exists.

Latent heat evolving from the condensing drop was assumed to be the major contributor to the dead space. Thus, if a source of heat could be introduced into the cloud chamber, a dead space about that source should exist. A wire of .04 inch diameter Trophet-A Nichrome was placed in the sensitive volume via one of the side ports. The wire was bent so that it dipped down into the water and came out of the water at the center of the chamber. It stood about 7 centimeters above the water level and perpendicular to it so that the wire appeared as a point when seen by the camera. A series of expansions were then performed ranging from medium to heavy fogs. The heat capacity

of the wire is sufficiently large that it remains at approximately 24° C, even though the sensitive volume temperature may be as low as -5° C.

This basic experiment showed a rather dramatic example of dead space, as shown in Plate 1. This picture was taken at supersaturation of about 5.5 and shows quite clearly that there exists a region about the wire in which no nucleation occurs. The dead space radius as measured is approximately .9 cm.

The same experiment was performed in argon. Since argon has a lower thermal conductivity, the dead space for argon should be smaller if heat is the major contributor. Plate 2 shows the result for argon. The measured value of dead space radius is approximately .3 cm.

2. A Theoretical Analysis of the Wire Experiment. Assuming heat the major cause of dead space in the wire experiment, one may make use of the heat diffusion equation:

$$K\left(\frac{d^2t}{dr^2} + \frac{1}{r}\frac{dt}{dr}\right) = \frac{dt}{d\tau} \quad , \qquad (4\text{-}1)$$

where K is the diffusion coefficient, t is the temperature, r is the radius, and τ is the time. Carslaw and Jaeger[24] do the problem in detail for cylindrical geometry and give a general solution that may be used. The boundary conditions are:

PLATE 1

PLATE 2

$$t(r,0) = t_0$$
$$t(a,\tau) = t' \qquad (4\text{-}2)$$
$$t(\infty,\tau) = t_0 \ ,$$

where a is the radius of the wire, t_0 is the temperature of the bulk vapor immediately after the expansion, and t' is the temperature of the wire. Choosing appropriate values of the diffusivity, wire radius, and time yields one of a family of curves representing the solution which are indexed by the quantity $K\tau/a^2$. From this curve the temperature of the bulk vapor at given distance from the wire may be found. Although the solution is exact, the value of the diffusivity of gases is in doubt since it varies with the temperature of the gas. Thus, the graphs shown in Fig. 6 for helium and Fig. 7 for argon are at best first approximations to the true solutions. The values of the diffusivity for both gases were taken at standard conditions.

In Fig. 6 and Fig. 7, graphs are shown for an expansion with final supersaturations at 5.6. The supersaturation at a specified distance from the wire or the temperature of the vapor at a specified distance from the wire is plotted. Below the line labelled S_{crit}, nucleation is negligible; above this line, it is measurable. The upper curve for both helium and argon shows the supersaturation profile at .065 seconds after the expansion, which is the time at the peak of the pulse. The lower curve for both Figures 6 and 7 shows the supersaturation at 0.3 sec. after the expansion, which is the time that Plates 1 and 2 were taken.

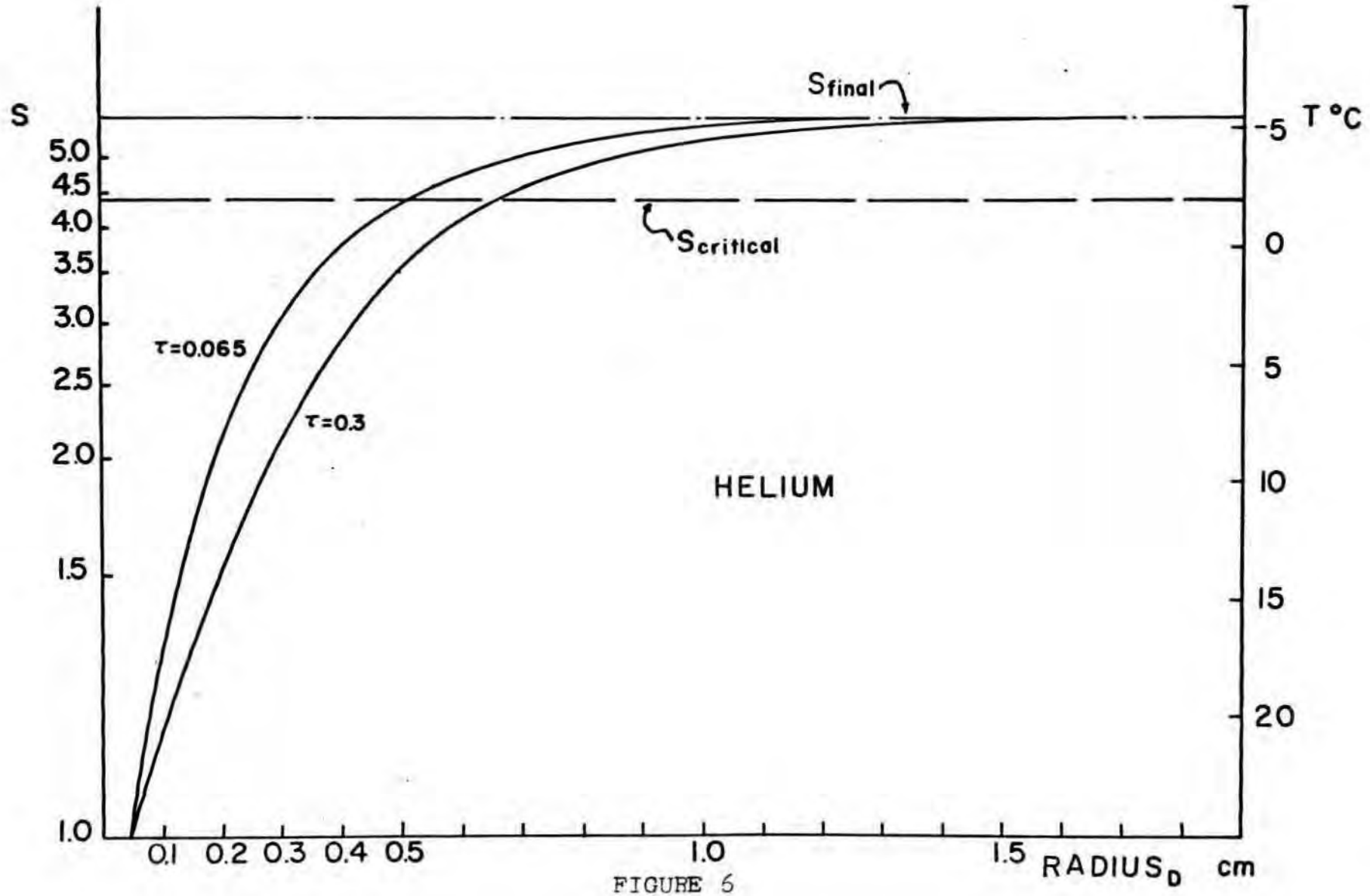
S
5.0
4.5
4.0
3.5
3.0
2.5
2.0
1.5
1.0
Sfinal
Scritical
τ=0.065
τ=0.3
HELIUM
T °C
-5
0
5
10
15
20
0.1 0.2 0.3 0.4 0.5
1.0
1.5
RADIUS$_D$ cm

FIGURE 6

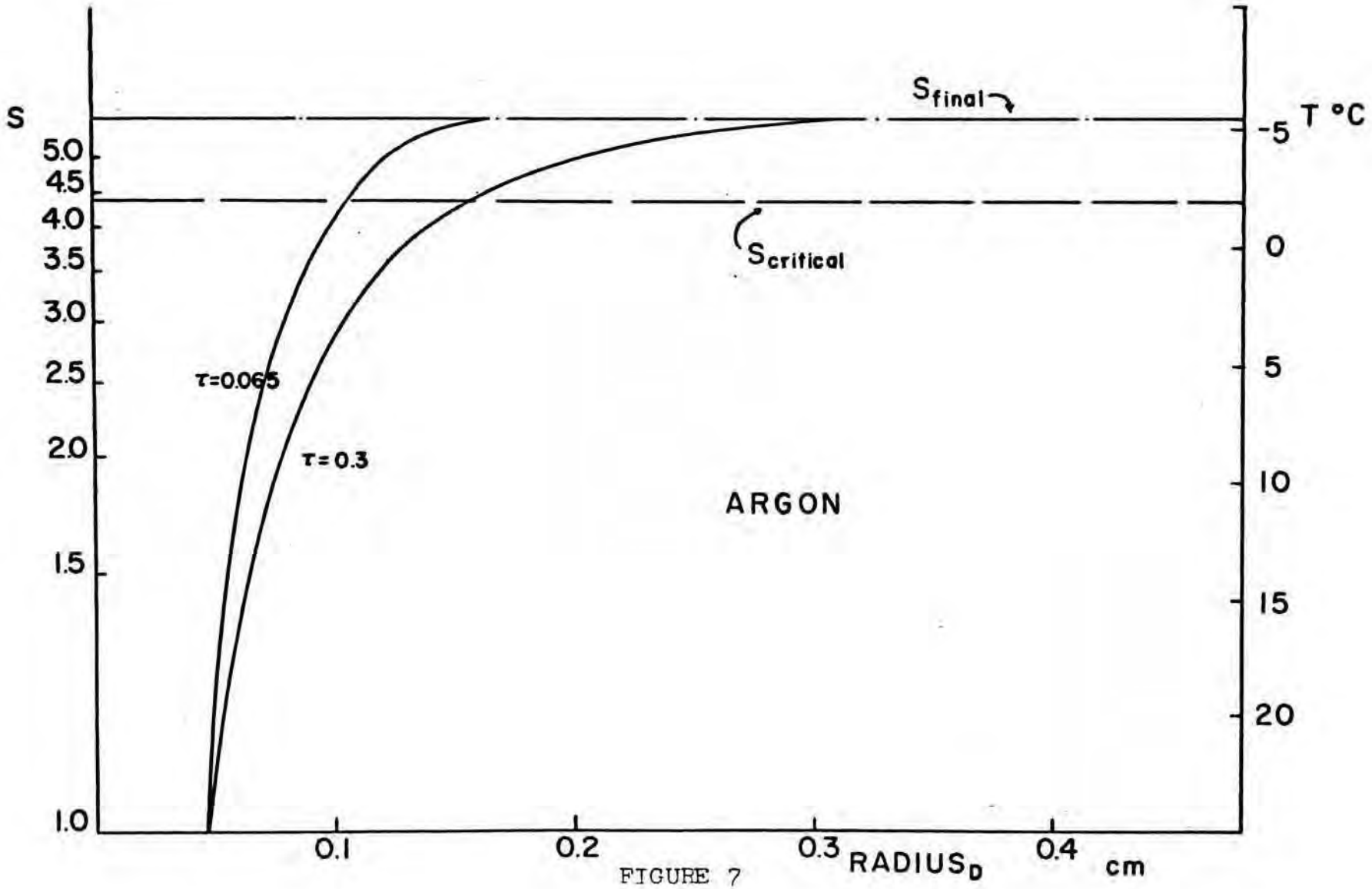
S
5.0
4.5
4.0
3.5
3.0
2.5
2.0
1.5
1.0
S_{final}
$S_{critical}$
τ=0.065
τ=0.3
ARGON
-5
0
5
10
15
20
T °C
0.1
0.2
0.3
0.4
RADIUS$_D$
cm

FIGURE 7

Thus, the intersection of the lower curve with S_{crit} marks the dead space radius as analyzed theoretically. For helium this is about .7 cm as compared to .9 cm measured, and for argon about .15 cm as compared to .3 cm measured.

Making use of Becker and Doring's nucleation rate, a profile of the number of drops nucleated in 0.3 seconds at different distances from the wire is plotted for helium, cf. Fig. 8, from the supersaturation profile in Fig. 6. This plot shows the same step function behavior as seen experimentally in Plates 1 and 2.

3. Double Pulse Expansions. This experiment consisted of two parts: 1) calibration run, 2) data run. The calibration run consists of a series of 10 to 15 single pulse expansions similar to the type used by Schmitt. The timing was adjusted so that all expansions in this run had approximately the same peak supersaturation. After drop counts and calculations were made, the drop count per cm^3 was plotted versus peak supersaturation for these expansions. This plot, shown in Fig. 9, served to establish the nucleation for a given pulse in a simpler fashion than that employed by Schmitt. This plot is used later.

The second part of the experiment consisted of double pulse expansions, an example of which is given in Fig. 10. The first pulse of this expansion is identical to that performed in the calibration run. The second pulse of the expansion was made so that it reached about the same peak

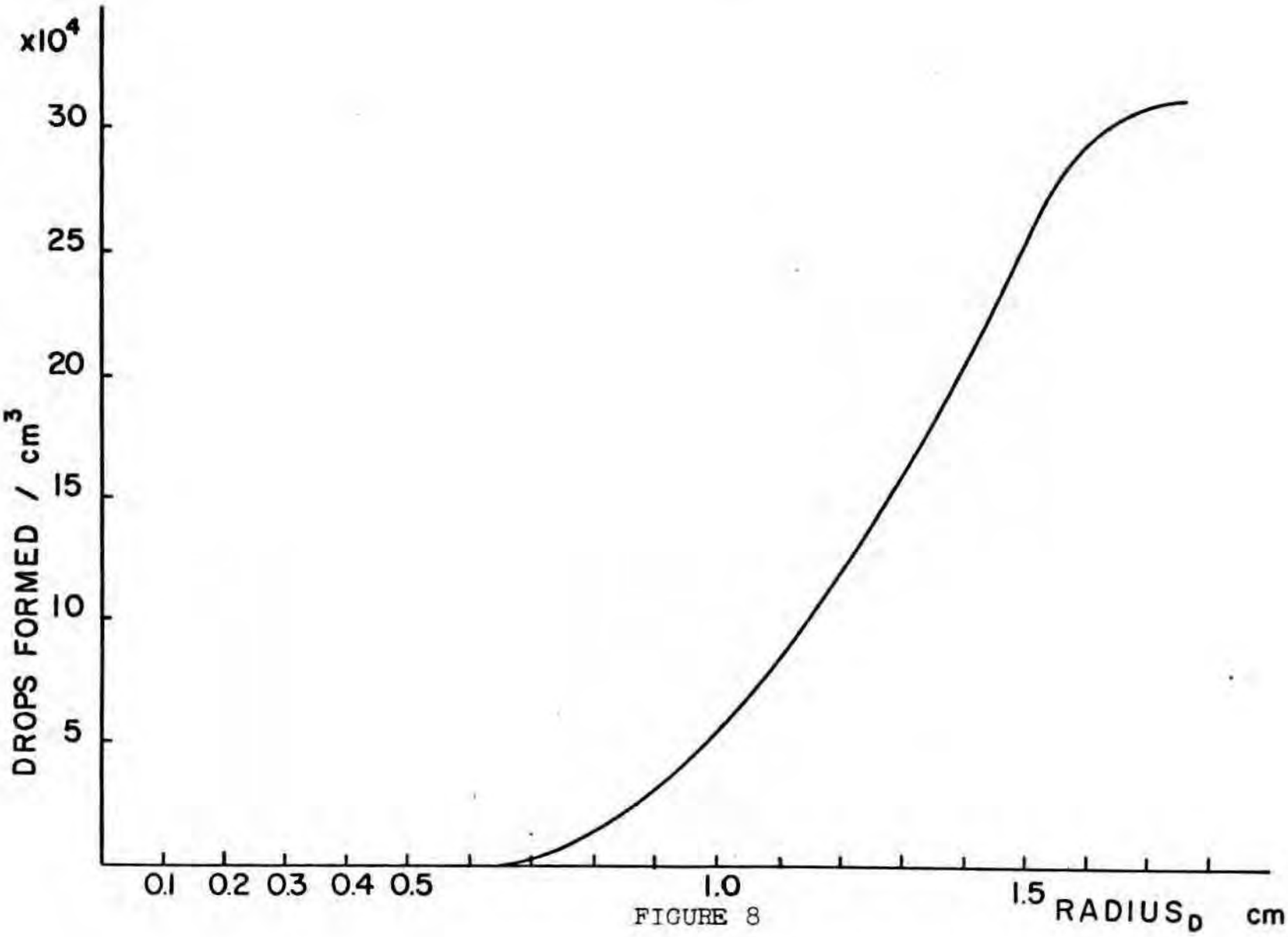
x10^4
30
25
20
15
10
5
DROPS FORMED / cm^3
0.1 0.2 0.3 0.4 0.5
1.0
1.5
RADIUS_D cm

FIGURE 8

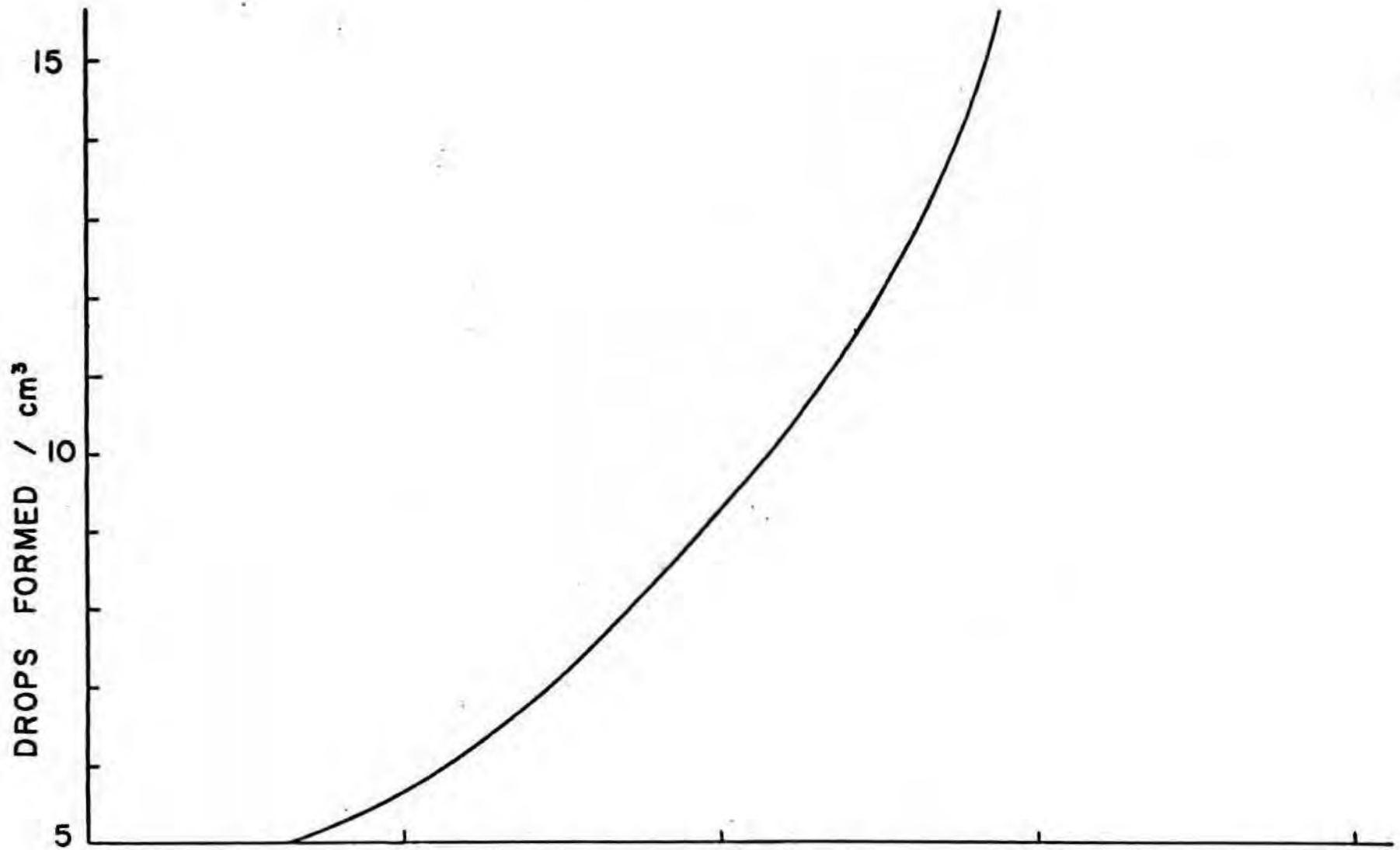

FIGURE 9

EXAMPLE OF DOUBLE-PULSE EXPANSION

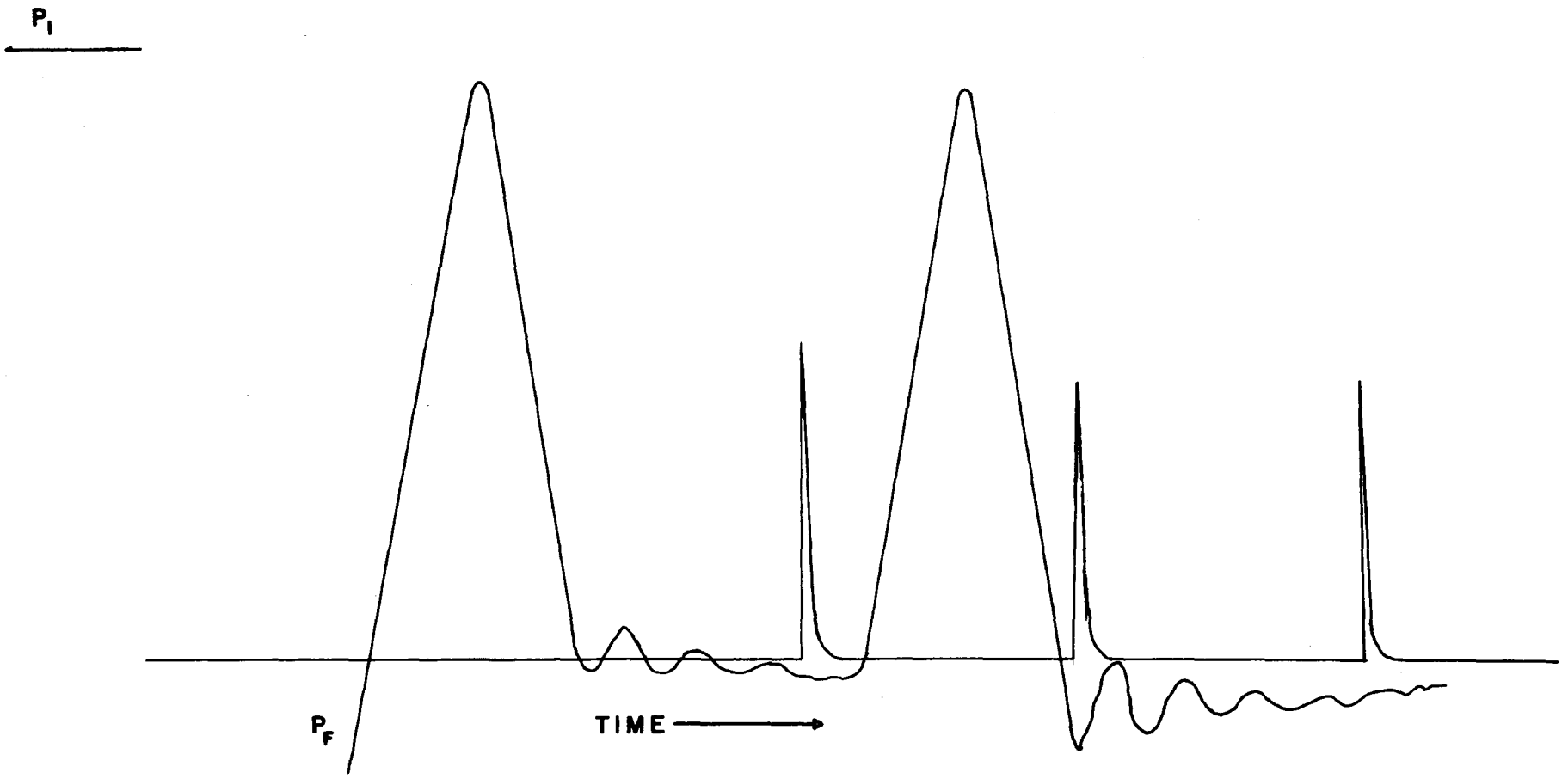

FIGURE 10

supersaturation as the first pulse. The time between the first and second pulses could be varied from 0.05 seconds to 0.50 seconds. Pictures were taken after the second pulse. In this fashion, droplets nucleated in the first pulse could grow so that their dead space would affect the number of drops nucleated in the second pulse. Since the time between pulses could be varied, the effect of dead space due to droplets nucleated during the first pulse could be measured with respect to droplet age.

4. Mathematical Analysis. The details of the analysis are quite straightforward. If N_0 is the number of drops/cm^3 observed for a double pulse, then:

$$N_0 = N_1 + \left[1 - D(t)N_1\right] N_2 \quad , \tag{4-3}$$

where N_1 is the number of drops/cm^3 nucleated under pulse one as taken from calibration run data, and N_2 is the number of drops/cm^3 nucleated under the second pulse taken from the same calibration curve, and D(t) is the dead space in cm^3/drop. The factor in brackets is the correction for that portion of the volume rendered "dead" by droplets from the first pulse. Eq. (4-1) may be solved for the quantity D(t),

$$D(t) = \frac{N_1 + N_2 - N_0}{N_1 N_2} \quad . \tag{4-4}$$

The various parameters have not been selected so that the gross effects of droplet growth override sufficiently

the random statistical nature of the nucleation process. The accuracy of a single drop count observation is $\pm\sqrt{N}$ where N is the total number of drops counted.[25]

If the number observed is greater than the number that should be nucleated by both pulses, then D(t) is meaningless. Thus, N_0 should be less than or equal to $N_1 + N_2$. This is observed in practice.

From Eq. (4-3) it is obvious that the quantity $D(t)N_1$ may be equal to unity but never greater than unity, otherwise N_2 would be negative, which is physically impossible. If one looks at the limiting case when $D(t)N_1 = 1$, then the second term in Eq. (4-3) is zero. Thus, $N_1 = N_0$ and the dead space per drop is simply:

$$D_1 = \frac{1}{N_1} \quad , \qquad (4\text{-}5)$$

where D_1 is the limiting dead space. Thus, the maximum observable dead space is a very definite function of the droplet density. If 10 drops/cm^3 are nucleated in the first pulse, then the largest dead space necessary per drop to render the cubic centimeter incapable of further nucleation is 0.1 cm^3. After D(t) becomes this large, the dead spaces of different droplets overlap and the concept of independent "dead spaces" becomes meaningless. For a hundred drops/cm^3 D_1 is 0.01 cm^3 per drop. Thus, for higher droplet densities, the maximum dead space per drop becomes smaller. From this analysis one has the limiting values that N_0 may take on for these experiments:

$$N_1 \leq N_0 \leq (N_1 + N_2) \quad . \qquad (4\text{-}6)$$

This is what one would expect physically, namely that the number of drops/cm^3 observed for the two pulses should be somewhere between the number nucleated in the first pulse and the number nucleated in both pulses, as taken from the calibrated data.

The analysis above assumes that for a single drop the nucleation about it varies as a step function with the distance from the drop. From the theoretical analysis in paragraph 2, one would expect it to vary in a continuous fashion. Figure 11 shows these two models superimposed. Note that the step function curve does not extend as far away from the drop as the diffusion curve. Thus, in actuality, droplets begin to compete with one another sooner than is indicated by the simple analysis involving D(t).

5. Other Details of the Experiment. Since the supersaturation for an expansion is very sensitive to small changes in the operating parameters, five double pulse expansions were taken with the time between the two pulses fixed. A second set of five expansions was taken with a different time between the two pulses, and so on for four different times out to about .25 seconds separating the two pulses. Several runs of this type were made and these resulted in data for droplet densities from 5 to about 30 drops/cm^3. Droplet densities higher than 30 drops/cm^3 are difficult to work with since a large amount of time is required for drop counting.

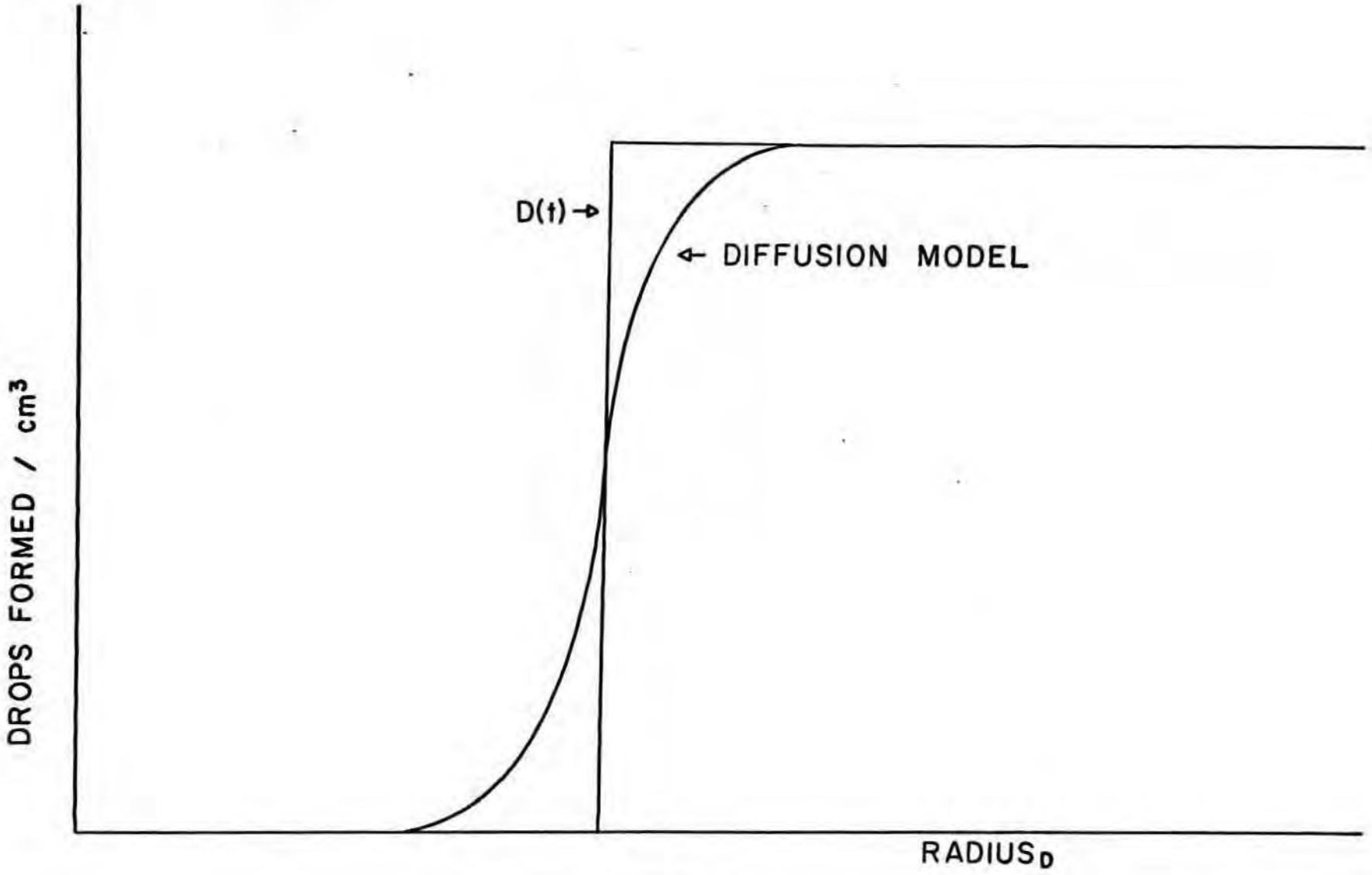

FIGURE 11

Peak supersaturations were always calculated. A computer program, the details of which are shown in Appendix A, performed the calculations of supersaturation.

Drop counts were done on four of the six frames taken by the stereoscopic camera. A volume from 10 to 64 cm^3 was counted, depending on droplet density, for each of the frames. The last four of the six frames were counted since the first two frames were taken too close to the second pulse to be of any value. The results of the drop counts were summed and averaged, then figured per cm^3. This procedure was followed in drop counting for both the calibration and data runs so that any systematic error would be duplicated in all cases.

With the peak supersaturations and drop counts, one has N_1, N_2, and N_0 and is able to perform the analysis given above for each series of runs. The data, as finally reduced, is shown in Fig. 12. The dead space in cm^3 per drop is plotted versus time. Each of the curves represents a certain drop density and is so labelled.

Since there is no way in which dead space may be measured by this technique for times less than .05 seconds, the effect of dead space on droplets nucleated in the first pulse itself is unknown. From the theoretical analysis done in paragraph 2, the actual dead space curve would look like the dashed line in Fig. 13, if dead space could be measured for very short times.

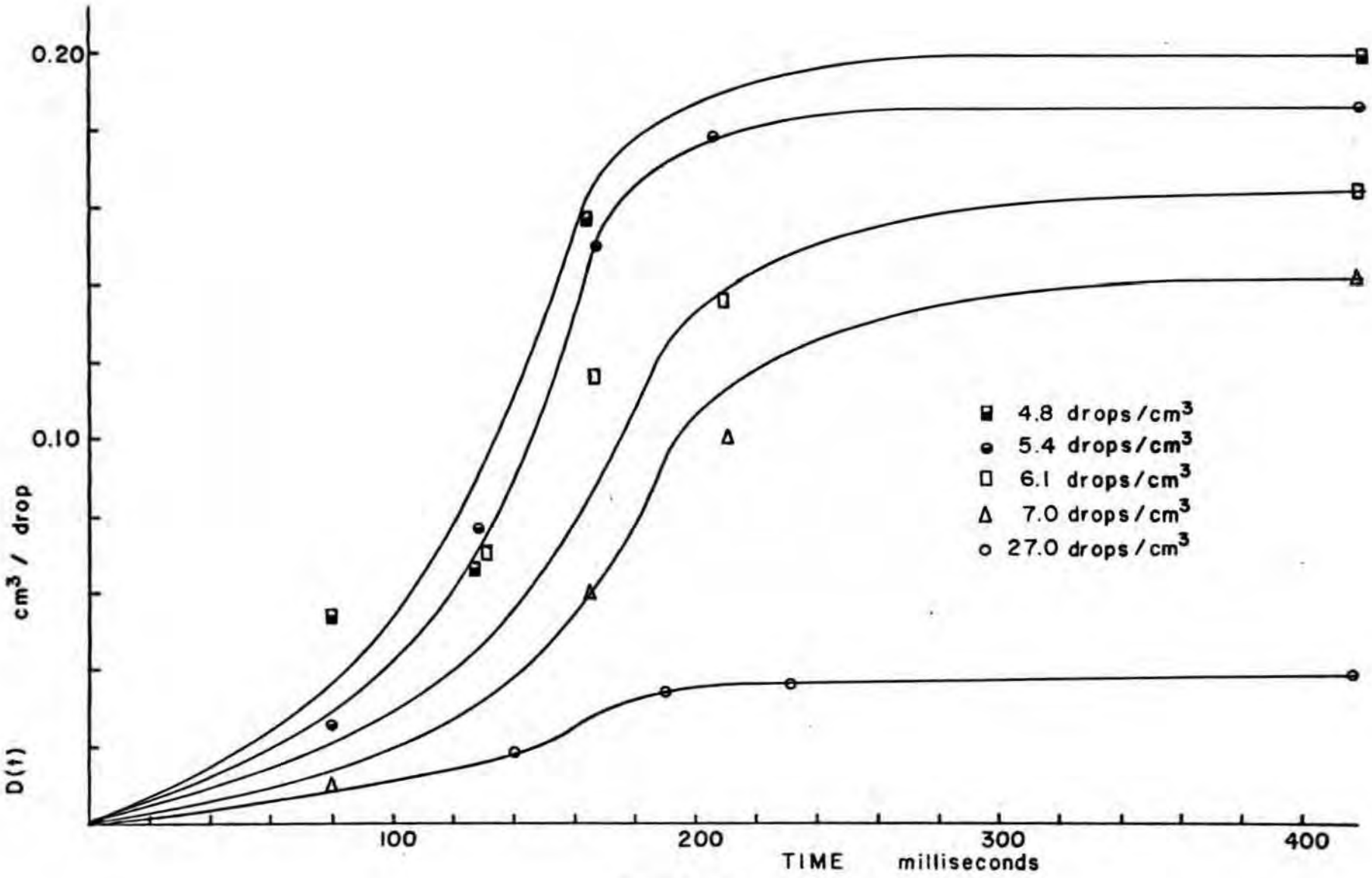
0.20
0.10
D(t)
cm³ / drop
100
200
300
400
TIME milliseconds
4.8 drops/cm³
5.4 drops/cm³
6.1 drops/cm³
7.0 drops/cm³
27.0 drops/cm³

FIGURE 12

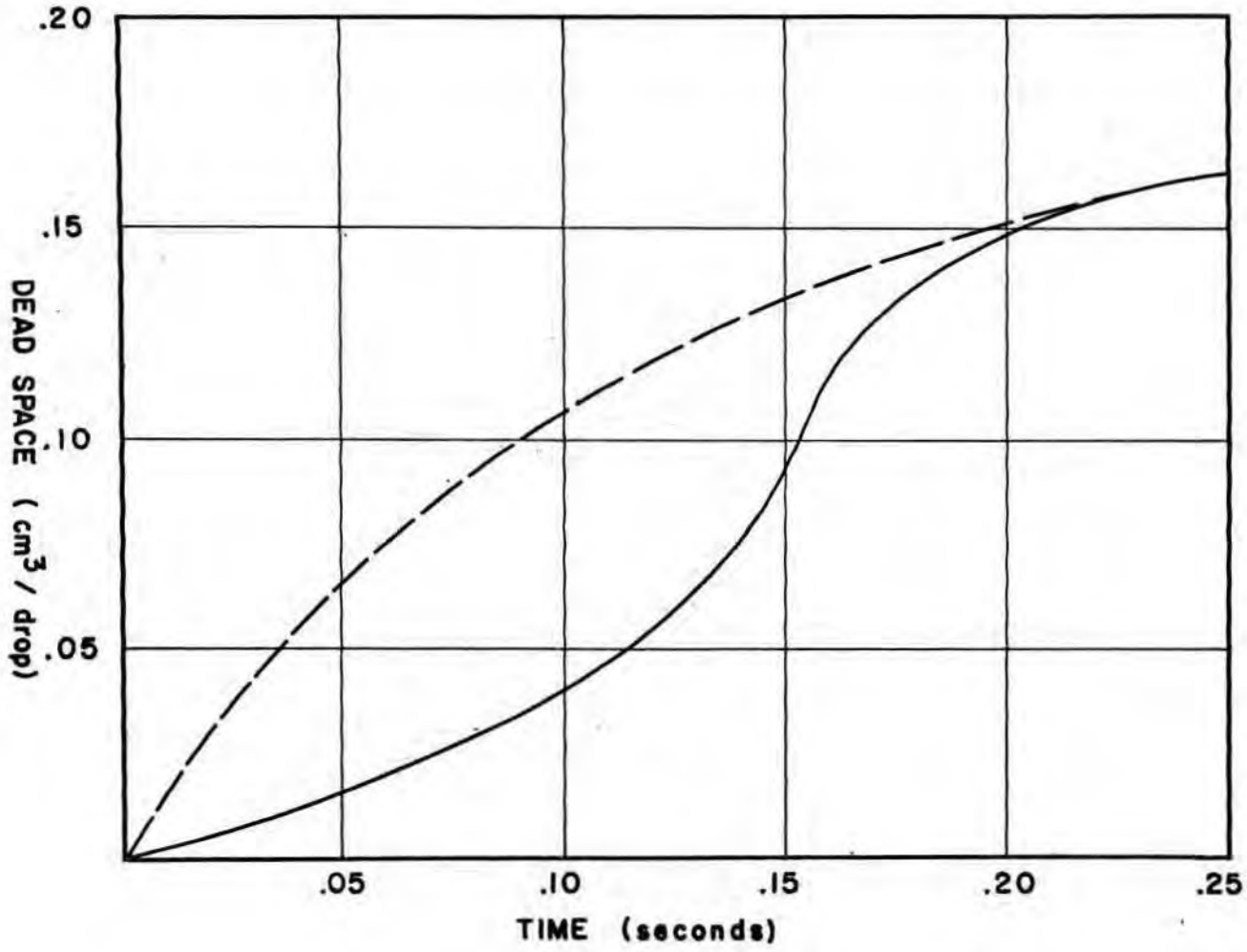

FIGURE 13

It has been shown by two different experiments and also from theory that a dead space does exist around growing droplets. This dead space is physically measurable and it is a major factor to be considered by those doing nucleation rate studies with the cloud chamber.

CHAPTER V

CONCLUSIONS

The results of this study show that future use of the cloud chamber as a tool for studying nucleation rates will have to make allowance for dead space effects.

1. Dead Space per Unit Volume. In order to visualize the effect of dead space on one cm^3 of the sensitive volume, a plot of percent dead space in a cm^3 versus time is shown in Fig. 14. The percent figure is obtained simply by multiplying D(t) times the drop densities from the information in Fig. 13. The result of this plot is to remove the dependence on droplet densities. Interestingly enough, this plot shows that for the drop densities studied, the percent dead space curve is almost the same. Thus, a density of 5 drops/cm^3 takes out about the same total dead space as a density of 30 drops/cm^3. This implies that a cm^3 of vapor at a supersaturation of 4.7 is not made dead appreciably faster than a cm^3 of vapor at a supersaturation of 5.0; this, despite the higher drop density of the latter case. This can be said only for those droplet densities studied, namely from 5 to 30 drops/cm^3.

2. Vapor Depletion. A cause of dead space present in the double pulse experiment is removal of water molecules from the vapor by nucleation and growing drops. The

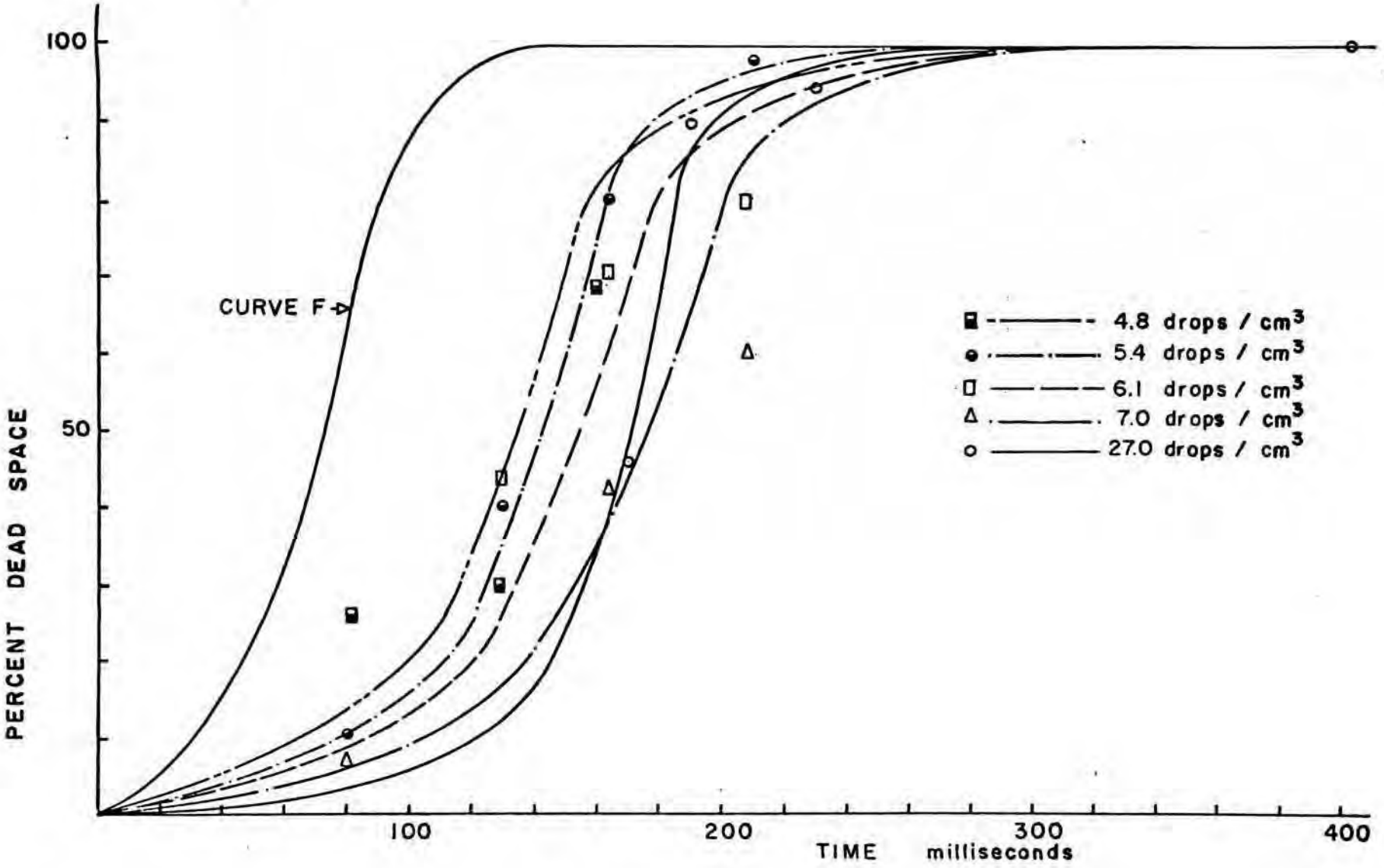
100
50
PERCENT DEAD SPACE
CURVE F
4.8 drops / cm3
5.4 drops / cm3
6.1 drops / cm3
7.0 drops / cm3
27.0 drops / cm3
100
200
300
400
TIME milliseconds

FIGURE 14

computer program is designed to measure the effect of vapor depletion in an approximate way. A series of square pulse expansions run on the computer show that at a droplet density of 10^3 drops/cm^3 vapor depletion effects commence about 0.1 seconds after the expansion. For droplet densities of 10^5 drops/cm^3 vapor depletion effects commence about .03 seconds after the expansion.

Thus, the dead space that has been measured in the cloud chamber by the double pulse expansion is in truth the result of two physical phenomena: 1) evolution of heat from the growing drop, and 2) removal of water molecules from the vapor by growing drops. The contribution to the dead space due to heat seems to predominate for low drop densities when vapor depletion effects are truly small. From the trend of percent dead space curves in Fig. 14 and the information above, one would expect the percent dead space curve for high droplet densities to be as shown by curve F in Fig. 14.

3. Further Work. In order to apply these results as corrections for empirically determined nucleation rates with the cloud chamber, the author proposes some topics for further study.

The method of numerical integration of expansions as performed by Schmitt should be done with two changes in procedure. First, cloud chamber expansions of the same maximum supersaturation should be performed with some means

of changing the width of the pulse. Second, the integration should also take into account dead space effects for each interval of the pulse, making use of the work presented above. Such an experiment would correct Schmitt's empirical curve for the effects of dead space.

Another worthwhile investigation would be to perform the experiment done by Schmitt with argon instead of helium. Preliminary studies by Dawbarn[26] show that for the same peak supersaturation, an expansion in argon yields approximately eight times as many drops nucleated as in helium. This startling result points up the fact that dead space does drastically affect cloud chamber measurements. The dead space for argon is considerably smaller then that for helium for drops of equal age. Thus, drops growing with argon as an inert gas do not perturb the sensitive volume as quickly or drastically as drops growing in helium. Consequently, rate determinations in argon may prove a worthwhile effort.

A last recommendation would be performing the experiment in a vacuum. Thus, effects of the inert gas would be removed altogether. This experiment would necessitate the building of a new piece of apparatus and would pose several difficult technical problems. However, it would minimize dead space effects on the homogeneous nucleation rate as determined with the cloud chamber.

BIBLIOGRAPHY

1. N. H. Fletcher, The Physics of Rainclouds, Cambridge: University Press, 1962.

2. C. T. R. Wilson, "Condensation of Water Vapor in the Presence of Dust-free Air and Other Gases," Phil. Trans. Roy. Soc. (London) A189, 265 (1897).

3. M. Volmer and A. Weber, "Nucleation in Supersaturated Systems," Z. Phys. Chem. 119, 277 (1926).

4. F. Frey, "On the Condensation of Vapor in an Inert Gas," Z. Phys. Chem. B49, 83 (1941).

5. W. G. Courtney, Kinetics of Condensation from the Vapor Phase, Summary Report TM-1250, Texas Experiment, Inc., 1961.

6. E. F. Allard and J. L. Kassner, "A New Cloud Chamber Method for the Determination of Homogeneous Nucleation Rates," Jour. Chem. Phys. 42, 1401 (1965).

7. F. J. M. Farley, "The Theory of Condensation of Supersaturated Ion-free Vapor," Proc. Roy. Soc. A212, 530 (1952).

8. H. Reiss, "Recent Developments in Nucleation Theory," Z. Elekchem. 56, 459 (1952).

9. Lord Kelvin, "On the Equilibrium of Vapor at a Curved Surface of Liquid," Proc. Roy. Soc. Edin. 7, 63 (1870).

10. F. P. Buff and G. Kirkwood, "Remarks on the Surface Tension of Small Droplets," Jour. Chem. Phys. 18, 991 (1950).

11. V. K. La Mer and G. M. Pound, "Surface Tension of Small Droplets from Volmer and Flood's Nucleation Data," Jour. Chem. Phys. 17, 1337 (1949).

12. H. R. Byers and S. K. Chary, "Surface Tension of Water Droplets at the Critical Radius," J. App. Math. and Phys. 14, 428 (1963).

13. R. Becker and W. Döring, "Kinetics of Nucleation in Supersaturated Vapors," Ann. der Physik 24, 719 (1935).

14. R. J. Schmitt, Masters Thesis, University of Missouri at Rolla, 1965.

15. L. Farkas, "Speed of Nucleus Formation in Supersaturated Vapor," Z. Phys. Chem. 125, 236 (1927).

16. J. Zeldovich, "Theory of the Formation of a New Phase," J. Exp. Theor. Phys. (Russian) 12, 525 (1942).

17. A. Sander and G. Damköhler, "Supersaturation in the Case of Spontaneous Nucleation in Water Vapor," Naturwissen. 31, 460 (1943).

18. J. Frenkel, Kinetic Theory of Liquids, Oxford: Oxford University Press, 1946.

19. E. Bagge, F. Becker, and G. Bekow, "The Growth Rate of Cloud Drops in the Wilson Cloud Chamber," Z. Ange. Physik 3, 6 (1951).

20. N. N. Das Gupta and S. K. Ghosh, "A Report on the Wilson Cloud Chamber and Its Applications in Physics," Rev. Mod. Phys. 18, 225 (1946).

21. International Critical Tables of Numerical Data, Physics, Chemistry, and Technology, New York: McGraw-Hill Book Company, Inc., 1926.

22. E. F. Allard, "A New Determination of the Homogeneous Nucleation Rate of Water in Helium," Ph. D. Dissertation, University of Missouri at Rolla, 1964.

23. D. L. Packwood, Masters Thesis, University of Missouri at Rolla, 1965.

24. H. S. Carslaw and J. C. Jaeger, Conduction of Heat in Solids, 2nd ed., Oxford: Oxford Press, 1959.

25. W. J. Price, Nuclear Radiation Detection, New York: McGraw-Hill Book Company, Inc., 1958.

26. R. Dawbarn, Masters Thesis, University of Missouri at Rolla, 1965.

APPENDIX A

The computer program shown here is designed to be as flexible as possible for not only this work but work done in the future. It consists of a mainline deck and three subroutines. The program is written in Fortran II and provisions have been made for storing the subroutines on a magnetic memory disc to facilitate its use.

The program performs one of two main calculations in one of three ways. The main calculations available are: 1) supersaturations and final temperatures, 2) supersaturations and an accounting for the number of water molecules per cm^3 removed by nucleation and growth. This information is applied at each interval as a correction for both the final supersaturation and the nucleation rate. Both calculations give the total number of drops nucleated under the pulse as done in Schmitt's numerical integration. This last calculation provides the user with the option to use any one of five rate laws, those being: Farley, Becker and Döring, Sander and Damköhler, Volmer, and Schmitt's empirical curve. If the user desires, he may program any or all of the other rate laws into subroutine PH300R.

The ways in which expansions may be calculated are three: 1) point by point data read from the final pressure trace, 2) pressure data from an internally generated

parabolic pulse, 3) pressure data from an internally generated square pulse. The choice of calculation is determined by the user.

The three subroutines are used to calculate the supersaturation, the number of molecules in a drop of critical radius, and the number of drops nucleated in a pulse. Data input to this program consists of four parts; 1) label, specifying the date, operator, experiment, and expansion number, 2) calibration data which calibrates the final and initial pressure scales, 3) the option card which enables the user to specify which calculation to be performed from what kind of pulse and using a specific rate law, 4) the initial pressure, final pressure, initial temperature, and sensitive time width. The data in part 4 is entered in various ways depending upon the form the final pressure pulse the user desires. The final program is shown below.

```
C       CENTRAL PROGRAM FOR CLOUD CHAMBER CALCULATIONS
C       SUBROUTINE PH300S (SUPERSATURATION)
C       SUBROUTINE PH300G (NUMBER OF MOLECULES PER DROP)
C       SUBROUTINE PH300R (NUCLEATION RATE)
        DIMENSION DRPNU(100),EMREM(100),VP(351),READN( 90)
        COMMON RSTAR,SIGMA,R,S,PI,GSTAR,APF,EMF,READN,BF,TO,DT,PCRIT,BO,
       1PMIN,TF,TI,GAM,VP,VPI,ID,AVNO,IRATE,CONST,AVNOR,PFUNC,CINST,API,
       1VPF,N,RATE
   10 FORMAT(5I1)
   11 FORMAT (F6.3,13F5.3)
   12 FORMAT (6F12.5)
  450 FORMAT (6I2)
  980 FORMAT (6E12.5)
        READ 11,(VP(J),J=1,351)
        READ 980,BO,SIGMA,PI,R,GAM,AVNO
        CINST=36.**.66666
        CONST=18.**1.66666
        AVNOR=AVNO**.33333
        PFUNC=PI**.33333
  300 READ 10,ID,IT,IM,IRATE,NDET
        PRINT 999
  999 FORMAT (1H1)
        IF(NDET-1)801,802,802
  801 READ 12,XI,YI,XF,YF,TI
        EMI=5.347
        EMF=5.564
        BI=YI-EMI*XI
        BF=YF-EMF*XF
  802 CONTINUE
        READ 450,LM,LD,LY,LOP,LEX,LSEQ
        PRINT 451, LM,LD,LY,LOP,LEX,LSEQ
  451 FORMAT (1X,5HDATE ,I2,1H/,I2,1H/,I2,2X,9HOPERATOR ,I2,2X,
       115HEXPERIMENT NO. ,I2,2X,14HEXPANSION NO. ,I2)
        IF(ID-1)50,51,52
   50 PRINT 55
   55 FORMAT(1X,32HPRESSURE DATA ENTERED FROM PULSE)
```

```
      GO TO 60
   51 PRINT 56
   56 FORMAT(1X,37HPRESSURE DATA GENERATED FROM PARABOLA)
      GO TO 60
   52 PRINT 57
   57 FORMAT(1X,41HPRESSURE DATA GENERATED FROM SQUARE PULSE)
   60 GO TO (401,402,403,404,410),IRATE
  401 PRINT 405
  405 FORMAT(1X,22HBECKER DORING RATE LAW)
      GO TO 400
  402 PRINT 406
  406 FORMAT(1X,17HVOLMER I RATE LAW)
      GO TO 400
  403 PRINT 407
  407 FORMAT(1X,25HSANDER DAMKOHLER RATE LAW)
      GO TO 400
  404 PRINT 408
  408 FORMAT(1X,15HFARLEY RATE LAW)
      GO TO 400
  410 PRINT 411
  411 FORMAT (1X,11HSCHMITT LAW)
  400 IF(ID-1)13,14,14
   13 READ 998,INT
  998 FORMAT(I2)
      READ 12,RAPI,(READN(N),N=1,INT),STW
      ENT=INT
      SDT=STW/ENT
      API=(EMI*RAPI+BI)*2.49E+03
      GO TO 15
   14 READ 12,RAPI,RCRIT,RMIN,TO
      INT=20
      ENT=INT
      SDT=TO/10.
      PCRIT=(EMF*RCRIT+BF)*2.49E+03
      API=(EMI*RAPI+BI)*2.49E+03
   15 IF(IT-1)20,21,21
```

```
 20 PRINT 61
 61 FORMAT(1X,21HSUPERSATURATIONS ONLY,10X,18HFINAL TEMPERATURES)
    SSUM=0.
    DO 22 L=1,INT
    EL=L
    DT=SDT*EL
    N=L
    CALL PH300S
    PRINT 62,S,TF
 62 FORMAT(1X,F6.3,25X,F12.5)
    CALL PH300G
    CALL PH300R
    DRPNU(L)=RATE*SDT
 22 SSUM=SSUM+DRPNU(L)
    PRINT 900,SSUM
900 FORMAT(1X,24HTOTAL DROPS NUCLEATED= ,F10.3)
    GO TO 100
 21 DT=SDT
    N=1
    PRINT 63
 63 FORMAT(2X,5HS NOM,3X,5HS ACT,4X,8HRATE NOM,4X,8HRATE ACT,4X,
   C8HMOLE.NOM,3X,13HTMREM TO DATE)
    CALL PH300S
    CALL PH300G
    CALL PH300R
    DRPNU(1)=RATE*DT
    EMREM(1)=DRPNU(1)*GSTAR
    TMREM=EMREM(1)
    ENSUM=EMREM(1)
    SN=S
    SA=S
    RATEN=RATE
    ARATE=RATE
    EMNOM=(SN*VPF)/(BO*TF)
    PRINT 64,SN,SA,RATEN,ARATE,EMNOM,TMREM
 64 FORMAT(2X,2(F6.3,2X),4(E10.3,2X))
```

```
      DO 25 L=2,INT
      EL=L
      DT=SDT*EL
      N=L
      CALL PH300S
      SN=S
      CALL PH300G
      CALL PH300R
      RATEN=RATE
      EMFIN=VPF/(BO*TF)
      EMNOM=SN*EMFIN
      EMCOR=EMNOM-TMREM
      S=EMCOR/EMFIN
      SA=S
      CALL PH300G
      CALL PH300R
      ARATE=RATE
      DRPNU(L)=ARATE*SDT
      EMREM(L)=DRPNU(L)*GSTAR
      GSUM=0.
      DO 30 M=1,L
      EM=M
      IF(EL-EM)32,32,31
   31 GSUM=GSUM+(DRPNU(M)*4.*PI*.239*(EMCOR-EMF)*8.E-08*((EL-EM)*SDT))
      GO TO 33
   32 ENSUM=ENSUM+EMREM(M)
   33 CONTINUE
   30 CONTINUE
      TMREM=GSUM+ENSUM
      PRINT 64,SN,SA,RATEN,ARATE,EMNOM,TMREM
   25 CONTINUE
      SUM=0.
      DO 40 N=1,INT
   40 SUM=SUM+DRPNU(N)
      PRINT 900,SUM
  100 CONTINUE
```

```
      IF(IM-1)66,67,67
   67 GO TO 300
   66 CALL EXIT
      END
```

```
      SUBROUTINE PH300S
      DIMENSION READN(90),VP(351)
      COMMON RSTAR,SIGMA,R,S,PI,GSTAR,APF,EMF,READN,BF,TO,DT,PCRIT,BO,
     1PMIN,TF,TI,GAM,VP,VPI,ID,AVNO,IRATE,CONST,AVNOR,PFUNC,CINST,API,
     1VPF,N,RATE
      IF(ID-1)1,2,3
    1 APF=(EMF*READN(N)+BF)*2.49E+03
      GO TO 4
    2 T=-TO+DT
      APF=((PCRIT-PMIN)*(T**2))/TO**2+PMIN
      GO TO 4
    3 APF=PMIN
    4 TF=TI/((API/APF)**((GAM-1.)/GAM))
      J=TI*10.-2631.
      VPI=VP(J)*1.332E+03
      K=TF*10.
      EK=K
      IF(TF*10.-EK-0.5)5,5,6
    5 J=TF*10.-2631.
      GO TO 7
    6 J=TF*10.-2630.
    7 VPF=VP(J)*1.332E+03
      S=(VPI*APF)/(VPF*API)
      RETURN
      END
```

```
      SUBROUTINE PH300R
      DIMENSION READN(90),VP(351)
      COMMON RSTAR,SIGMA,R,S,PI,GSTAR,APF,EMF,READN,BF,TO,DT,PCRIT,BO,
     1PMIN,TF,TI,GAM,VP,VPI,ID,AVNO,IRATE,CONST,AVNOR,PFUNC,CINST,API,
     1VPF,N,RATE
      Z=(VPI*APF)/(BO*API*TF)
      EXFA1=((SIGMA/TF)**3)*(18.**2)
      EXFA2=(16.*PI*AVNO)/(3.*(R**3)*((LOGF(S))**2))
      DENFA=EXPF(EXFA1*EXFA2)
      GFUNC=GSTAR**.33333
      GO TO (501,502,503,504,505),IRATE
  501 O1=1.
      CA=2.*Z*VPF*SIGMA*O1*18.*AVNO
      CB=3.*LOGF(S)*((R*TF)**2)*GSTAR
      CC=SQRTF((SIGMA*AVNO)/(PI*18.))
      RATE=((CA/CB)*CC)/DENFA
      GO TO 500
  502 CA=2.*VPF*SIGMA*CONST*AVNOR*Z
      CB=3.*(LOGF(S))*(R**2)*(TF**2)*GFUNC
      CC=SQRTF((2.*CINST*SIGMA*AVNO)/(18.*PFUNC))
      CD=EXPF((7.4E-13)/(BO*TF))
      RATE=((CA/CB)*CC*CD)/DENFA
      GO TO 500
  503 CA=Z*VPF*SIGMA*CONST*AVNOR
      CB=6.*(LOGF(S))*(R**2)*(TF**2)*GFUNC
      CC=SQRTF((2.*CINST*SIGMA*AVNO)/(18.*PFUNC))
      CF=(1.-(4./(GFUNC**2))+(2./GSTAR))
      DNFA=EXPF(EXFA1*EXFA2*CF)
      RATE=((CA/CB)*CC)/DNFA
      GO TO 500
  504 CA=(Z*VPF*18.)/(R*TF)
      CB=SQRTF((2.*SIGMA*AVNO)/(PI*18.))
      RATE=(CA*CB)/DENFA
      GO TO 500
  505 SL=-38.547+10.9167*S-.619494*(S**2)+.816435*(S**3)-.291291*(S**4)
     C+.0260969*(S**5)
```

```
      RATE=(10.**SL)*10.
  500 CONTINUE
      RETURN
      END
```

```
      SUBROUTINE PH300G
      DIMENSION READN(90),VP(351)
      COMMON RSTAR,SIGMA,R,S,PI,GSTAR,APF,EMF,READN,BF,TO,DT,PCRIT,BO,
     1PMIN,TF,TI,GAM,VP,VPI,ID,AVNO,IRATE,CONST,AVNOR,PFUNC,CINST,API,
     1VPF,N,RATE
      RSTAR=(36.*SIGMA)/(R*280.*LOGF(S))
      GSTAR=(4.*PI*(RSTAR**3))/(8.96E-23)
      RETURN
      END
```

APPENDIX B

The values of the constants taken for evaluating the quantities A and B in the rate laws studied in Chapter II are listed below.

$Z_1 \cong 10^{17}$ molecules/cm^3

$P_1 \cong 10^3$ dynes/cm^2

$M = 18.0$

$\sigma = 75$ dynes/cm^2

$N_0 = 6.025 \times 10^{23}$ molecules

$S = 5.0$

$R = 8.317 \times 10^7$ ergs/(gm-mole)-°K

$T = 268°$ Kelvin

$g \cong 100$ molecules

$\rho = 1$ gm/cm^3

$O_K = 46.7 \times 10^{-16}$ cm^2

$O_1 = 78.5 \times 10^{-16}$ cm^2

The results for evaluating the constants A and B are shown in the table below.

Author	A	B
Becker and Döring	6.75×10^{24}	125
Zeldovich	$\gamma 6.75 \times 10^{24}$	125
Farkas	$c1.44 \times 10^{22}$	125
Sander and Damköhler	3.38×10^{24}	105
Volmer	2.65×10^{26}	125
Frenkel	3.89×10^{26}	125
Farley	1.03×10^{24}	125

These are the values of A and B used to obtain the plots in Fig. 2.

VITA

The author was born July 18, 1941, the son of America and Hugh Grayson. The first eight years of his education were at St. Peter's Parochial School in Laredo, Texas, Our Lady of the Lake Grade School in San Antonio, Texas, and Immacolata Grade School in Richmond Heights, Missouri. He attended De Andreis High School in St. Louis, Missouri, graduating in June of 1959. He then attended St. Louis University for four years, receiving the Bachelor of Science Degree, Physics Major, in June of 1963. In the fall of 1963, he entered the University of Missouri at Rolla.